Remote Sensing of Environment 318 (2025) 114557

Contents lists available at ScienceDirect

Remote Sensing of Environment

journal homepage: www.elsevier.com/locate/rse

A geostatistical approach to enhancing national forest biomass assessments with Earth Observation to aid climate policy needs

Neha Hunka [a,*], Paul May [b], Chad Babcock [c], José Armando Alanís de la Rosa [d], Maria de los Ángeles Soriano-Luna [d], Rafael Mayorga Saucedo [d], John Armston [a], Maurizio Santoro [e], Daniela Requena Suarez [f], Martin Herold [f], Natalia Málaga [f], Sean P. Healey [g], Robert E. Kennedy [h], Andrew T. Hudak [i], Laura Duncanson [a]

[a] *Department of Geographical Sciences, University of Maryland, 4600 River Road, Riverdale, 20737, MD, USA*
[b] *Department of Mathematics, South Dakota School of Mines and Technology, Rapid City, 57701, SD, USA*
[c] *Department of Forest Resources, University of Minnesota, St. Paul, 55108, MN, USA*
[d] *Comisión Nacional Forestal (CONAFOR), Zapopan, 45019, Jalisco, Mexico*
[e] *GAMMA Remote Sensing Research and Consulting AG, Worbstrasse 225, Gümligen, Switzerland*
[f] *Helmholtz Center Potsdam GFZ German Research Centre for Geosciences, Remote Sensing and Geoinformatics, Telegrafenberg, 14473, Potsdam, Germany*
[g] *US Forest Service, Rocky Mountain Research Station, 84405, UT, USA*
[h] *College of Earth, Ocean, and Atmospheric Sciences, Oregon State University, Corvallis, 97331, OR, USA*
[i] *US Forest Service, Rocky Mountain Research Station, 83843, ID, USA*

ARTICLE INFO

Edited by Marie Weiss

Keywords:
Earth observation
National forest inventory
ESA CCI biomass
NASA GEDI
Geostatistical model
Climate policy
Mexico

ABSTRACT

Earth Observation (EO) data can provide added value to nations' assessments of vegetation aboveground biomass density (AGBD) with minimal additional costs. Yet, neither open access to global-scale EO datasets of vegetation heights or biomass, nor the availability of computational power, has proven sufficient for their wide uptake in climate policy-related assessments. Using Mexico as an example, one of the primary obstacles to enhancing their National Forest Inventory (NFI) with such global EO datasets is the lack of statistically defensible methodologies that do so, while addressing the nation's existing reporting needs and gaps. In collaboration with the Comisión Nacional Forestal (CONAFOR), this study develops a geostatistical model that integrates vegetation height and AGBD estimates from NASA's Global Ecosystem Dynamics Investigation (GEDI) and ESA's Climate Change Initiative (CCI) with Mexico's NFI to attain sub-national and geographically-explicit biomass predictions. The posited model includes spatially varying parameters, allowing flexibility to capture non-stationary relations between the EO-based covariates and NFI-estimated AGBD. Inference is conducted with Bayesian methods, allowing the computation of summary statistics, such as the standard deviations for single-location and area-wide predictions of AGBD. This enables the transparent disclosure and traceability of sources of uncertainty throughout the prediction approach. Results indicate strong model performance; the EO-based covariates explain 79% of the variance in NFI-estimated AGBD in a randomly withheld sample of 10% of observations and a heuristic root mean squared error (RMSE) of 21.55 Mg/ha. Approximately 96% of the observations falling within the 95% credible intervals of our predictions, with some systematic under-prediction observed at AGBD ranges of > 100 Mg/ha. To ease the operational uptake of the model for policy purposes, source code based in the 'R' language with the optional use of urban and (non)forest masks for AGBD predictions is released. It includes demonstrations for predicting AGBD in Mexico's Natural Protected Areas, terrestrial ecological strata, and community forest management or payment for environmental services projects, which are commonly used delineations in its climate policy reports. For other nations considering the presented approach for policy purposes, the study discusses challenges concerning the use of EO-based covariates and the limitations of the model. It concludes with a broader call toward ensuring consistency in EO data streams, and prioritizing the co-development of EO-NFI integration approaches with nations in the future, thereby directly addressing their long-term climate policy needs.

* Corresponding author.
E-mail address: nhunka@umd.edu (N. Hunka).

https://doi.org/10.1016/j.rse.2024.114557
Received 29 July 2024; Received in revised form 6 November 2024; Accepted 2 December 2024
Available online 11 December 2024
0034-4257/

1. Introduction

Forest biomass is recognized as an Essential Climate Variable by the Global Climate Observing System (GCOS, 2022), and its monitoring is critically important to climate change mitigation strategies and activities. Core elements of the Paris Agreement under the action of the United Nations Framework Convention on Climate Change (UNFCCC), directly or indirectly rely on biomass assessments to gauge nations' progress toward commitments to the reduction of land greenhouse gas emissions (UNFCCC, 2015). For example, emissions and removals of forest carbon, which is derived directly from forest biomass, in the land use, land-use change, and forestry sector are included in Biennial Transparency Reports (Art. 13, ibid.) submitted to the UNFCCC. These assessments may consequently be used as quantitative indicators for accounting of Nationally Determined Contributions (Art. 4, ibid.) (Melo et al., 2023). Several nations compile forest reference emission levels/forest reference levels under the Reducing Emissions from Deforestation and forest Degradation (REDD+) framework (UNFCCC, 2014). Aside from national commitments, various entities participate in voluntary, performance-based payment schemes tied to sub-national projects on REDD+ (Börner J. West et al., 2018; Streck, 2021). Irrespective of the path chosen toward climate change mitigation, a common policy-relevant necessity is to use accurate and consistent methodological approaches when estimating forest biomass. These methodological approaches must be both statistically rigorous and defensible by reporting teams, meeting the high level of transparency mandated by the UNFCCC and other reporting mechanisms. Without these considerations, parties can face challenges in technical reviews and/or audits related to biomass assessments.

National Forest Inventories (NFIs) are the main source of information on (sub)national forest biomass (Tomppo et al., 2010; Nesha et al., 2022; Melo et al., 2023). The estimation of area-wide mean aboveground dry woody biomass density (AGBD), often follows design-based protocols that are dependent on a probability sample of field plots located across the domain of interest (e.g., extent of a country). For design-based protocols, however, regularly maintaining field plot inventories is often logistically and financially prohibitive over vast or remote landscapes (Romijn et al., 2012). The recognition of this hurdle has encouraged scientific research toward the use of independently constructed global Earth Observation (EO) datasets (such as vegetation height, cover or AGBD map estimates) to augment ground-based national inventories. Using appropriate statistical procedures, EO datasets serve as auxiliary information to ground observations, enabling the scaling of estimates spatially, and increasing precision over small areas or of area-wide estimates (e.g. McRoberts, 2010; Ståhl et al., 2016; Babcock et al., 2018; Breidenbach et al., 2021; Emick et al., 2023). Of the available EO datasets for this purpose, light detection and ranging (lidar) from air- or space-borne sensors can provide accurate vegetation height and canopy density estimates that are correlated to biomass (Lefsky et al., 2002; Wulder et al., 2008; Duncanson et al., 2022). In the case of space-borne sensors, data acquired by National Aeronautics and Space Administration's (NASA) Global Ecosystem Dynamics Investigation (GEDI) from aboard the International Space Station are openly available for the period 2019–2023 for most temperate and tropical countries (Dubayah et al., 2020, 2022a). To overcome the partial spatial coverage of GEDI footprint-level data, wall-to-wall gridded estimates of vegetation height are often generated in combination with indices derived from optical or synthetic aperture radar (SAR) data (e.g. Potapov et al., 2021; Lang et al., 2023; Qi et al., 2023). Similarly, the European Space Agency's (ESA) Climate Change Initiative (CCI) has released vegetation AGBD maps generated with data from SAR satellites (Santoro et al., 2024), aided by data from the Ice, Cloud and land Elevation Satellite (ICESat −2) lidar mission (Markus et al., 2017). As more such open-science products are made available, efforts toward their incorporation in (sub)national AGBD assessments are a logical progression in the science of forest monitoring (Herold et al., 2019; GFOI, 2020).

In the choice of methods leveraging relationships between field observations and EO datasets, statistical rigour is of foremost importance to ensure compliance with standards mandated by policy; *good practices* in the Intergovernmental Panel on Climate Change (IPCC) Guidelines for National Greenhouse Gas Inventories stipulate that inventories with statistical inference must (i) "contain neither over nor under-estimates as far as can be judged" in which (ii) "uncertainties are reduced as far as practicable" (IPCC, 2006, 2019). Across domains that have a probability sample of observations, model-assisted estimators provide a rigorous approach to incorporating auxiliary information into a design-based estimation framework through an assisting model (Næsset et al., 2011; Ståhl et al., 2016; Ekström and Nilsson, 2021; Málaga et al., 2022). However, partial or incomplete NFIs are a common occurrence in tropical countries, where the timely and regular update of NFIs is often a constraint (Nesha et al., 2022). Such gaps in NFIs often invalidate design-based assumptions of random, probability samples. Instead, across domains that have few field plots, where probabilistic samples have not been acquired or gaps in sampling frames exist, model-based inference has been demonstrated as an alternative (e.g. McRoberts et al., 2014; Ståhl et al., 2016; Saarela et al., 2018; McRoberts et al., 2019). Rather than relying on the design of sampling locations, the validity of inference is determined by the model's distributional assumptions (Dumelle et al., 2022; McRoberts et al., 2022; Ståhl et al., 2024). As observations of a spatially continuous phenomenon (i.e. NFI-estimated AGBD at the NFI plot locations) in close proximity tend to exhibit similar values, studies have further employed *geostatistical* techniques within model-based frameworks to strengthen the validity of statistical inference. Herein, rather than assuming independent and identically distributed model errors, for example, spatially varying model parameters are defined to explicitly accommodate for residual spatial autocorrelation (e.g. Babcock et al., 2015, 2018; Emick et al., 2023; May et al., 2023). Thereby, geostatistical model-based (GMB) approaches enable spatially-continuous predictions of the phenomenon at locations where data are lacking, such as individual unvisited NFI plots or under-sampled areas. When inference is based in a Bayesian framework, predictions take the form of *posterior distributions*: probability distributions depicting knowledge of the unknown quantity given the observed data and model assumptions. From the posterior distributions, interpretable summaries can be computed, such as expected values, standard deviations (SDs) and 95% credible intervals (CIs). Predictions and uncertainties at the native resolution of the model (here, at the NFI plot-level) can be explicitly propagated to predictions and uncertainties for area-wide AGBD means. These aspects of Bayesian inference in model-based approaches are particularly advantageous for policy-related validation and verification processes, where the sources of uncertainty can be traced, and transparent reporting is critical to prove credibility.

Borrowing strength from auxiliary data to generate spatially-continuous predictions of spatially-sparse observations is a familiar concept in statistics, with applications in fields ranging from atmospheric sciences to public health. However, despite their relevance to forest biomass assessments, national policy-relevant applications of methods such as GMB remain largely absent to date. This gap may partially be attributed to the novelty of some EO datasets (e.g. GEDI-based vegetation heights are relatively new as of 2024), but a few other important challenges have been hurdles. First, geostatistical techniques have not been demonstrated to in-country technical teams in a manner that is easily replicable for operational use. Key takeaways from country consultations, for example through the U.S. Geological Survey SilvaCarbon program (USGS, 2012), have indicated that it is a substantial challenge to defend statistical models without supporting explanatory notes and open source code to implement them. Second, and closely related, analyzing spatial information using geostatistical techniques is computationally intensive; models that rely on AGBD observations at NFI plots must process spatial covariance matrices that grow quadratically in size as the number of plots increase across the domain of interest. Geostatistical techniques are often avoided simply due to their relative complexity to design-based or model-assisted approaches. Within the past two decades, substantial research has been dedicated to making geostatistical techniques feasible with large sample sizes, hence partially circumventing the computational burden (Heaton et al., 2019). Although many of these alternatives are now executable with packages in common statistical software, clear and transparent communication of their operational use and limitations is still lacking (Fassnacht et al., 2023). Third, supportive guidance with which countries may assess the potential integration of EO datasets in policy-relevant reports, such as those submitted to the UNFCCC, is absent (Herold et al., 2019; Melo et al., 2023; Hunka et al., 2023). As research in the use of EO datasets for forest biomass assessments collectively advances, international coordination bodies such as Global Forest Observations Initiative are recognizing the need for demonstrating EO-and-NFI data integration approaches. In parallel, the Committee on Earth Observation Satellites Biomass Harmonization activity (NASA, 2021), supported by the NASA's Carbon Monitoring System (NASA, 2010), has promoted direct collaboration with in-country greenhouse gas reporting teams to ensure transparency in methods toward increased uptake for policy initiatives.

In collaboration with the Comisión Nacional Forestal (CONAFOR), this study leverages the strengths of two EO-derived datasets to enhance Mexico's (sub)national forest AGBD assessments for climate policy reporting purposes. Despite an advanced forest inventorying system in place since 2004 (INFyS, 2024), the 3rd NFI cycle of Mexico is currently incomplete, which poses challenges to localized project-level or regional-scale biomass assessments. The study integrates NFI-estimated AGBD with open source datasets of (1) vegetation heights estimated from NASA GEDI (Dubayah et al., 2021; Potapov et al., 2021) and (2) AGBD estimated by ESA CCI Biomass (Santoro and Cartus, 2023). First, it develops a computationally-efficient geostatistical model to integrate the aforementioned datasets over the extent of Mexico, capitalizing on Bayesian inference to explicitly conduct an uncertainty estimation. Second, it demonstrates how the model results can be directly applied to obtain single-location and regional area-wide AGBD estimates. Within the article, demonstrations of assessments relevant to Mexico's policy needs are exemplified by (1) gap-filling locations of unvisited NFI plots with AGBD predictions and (2) predicting AGBD over arbitrary regions, such as nationally demarcated protected areas, terrestrial ecological strata, and projects of community forest management and payment for environmental services. With the forethought of the need for methods to be justifiable by policy reporting teams, and comprehensible to reviewers, the study presents an operationally-feasible methodology in accordance with FAIR (findable, accessible, interoperable, and replicable) principles (Wilkinson et al., 2016). An emphasis is placed on clarity of the statistical approach undertaken, supported by open source code with demonstrated use of the model.

2. Methods

2.1. Study area and datasets

2.1.1. National forest inventory

Our study domain is the extent of Mexico (∼196 Mha; between latitudes 32° and 14°N), covering a range of vegetation types in arid lands, dry temperate and tropical forests, mountain ecosystems and moist rainforests. CONAFOR maintains and measures a nationwide systematic gridded network of permanent plots as a part of the Inventario Nacional Forestal *y* de Suelos (INFyS) every five years. Grids range from 5 km × 5 km in temperate and tropical forests, 10 km × 10 km in dry and semi-arid vegetation and 20 km × 20 km in arid vegetation strata, and are continuous over vegetated and non-vegetated areas. However, due to various financial and logistical constraints, only 10,959 of the 26,220 proposed NFI locations were sampled in the 3rd NFI cycle between 2015 and 2019, resulting in spatially-irregular, non-random gaps in the probability design across the domain (Fig. 1). Where field visits were conducted, each NFI sample plot covered a circle with a radius 56.42 m (area of ∼1 ha), with four sub-plots of area 0.04 ha each. Trees with a diameter at breast height (DBH, 1.3 m) ≥ 7.5 cm were measured in each subplot. Species- and genus-specific allometric models and wood densities developed for Mexican forests were used to estimate tree-level AGBD, total subplot-level AGBD, and a ratio estimator was used to extrapolate to plot-level AGBD estimates (Velasco Bautista et al., 2020; CONAFOR, 2017; Urbazaev et al., 2018; Schroeder et al., 2012). The geostatistical model presented in this study is constructed using the plot-level AGBD estimates. The native resolution of the model is hence the size of the NFI plots (radii 56.42 m), and hereafter all NFI locations refer to areas of NFI plot size.

2.1.2. Earth observations maps

The two EO datasets – vegetation heights estimated from NASA GEDI and AGBD estimated by ESA CCI Biomass – were sourced directly from the data providers through publicly available portals, and are described below.

1. The GEDI lidar instrument was designed to provide high-precision estimates of vegetation height and structure between ± ∼ 51.6° latitudes since 2019. Relative Height (RH) metrics, i.e. the percentile of energy return height relative to the ground from full waveforms of laser pulses, are provided as discrete ∼25-m footprints in the GEDI L2 A product (Dubayah et al., 2021). To extend footprint-level data to continuous maps of vegetation height, they are commonly calibrated with wall-to-wall EO datasets. To acquire a product with vegetation heights estimated approximately over the dates of the 3rd NFI cycle in Mexico, we use the (Potapov et al., 2021) dataset. This dataset integrates GEDI acquisitions from April–October 2019 with year 2019 Landsat analysis-ready time-series data. The wall-to-wall Global Forest Canopy Height (2019) estimates were downloaded from the publicly available Global Land Analysis and Discovery portal and hereafter referred to as GEDI-based vegetation heights.
2. The CCI biomass dataset (version 4.0) includes a wall-to-wall mapped estimates of woody vegetation AGBD, in pixels of ∼1 ha, representing the year 2020 (Santoro and Cartus, 2023). To create the map, metrics of canopy height and density from ICESat GLAS and sub-national averages of canopy height from ICESat −2 and AGBD compiled from various NFI reports are first related in two allometric models. The parameters estimated in these models are then used as direct inputs in a physics-based semi-empirical model that relates AGBD to data from SAR backscatter, obtained from the Advanced Land Observing Satellite 2 Phased Array L-band SAR 2 and the Sentinel-1 A and -1B satellites (Santoro et al., 2024). As backscatter sensitivity to AGBD varies drastically with seasonal conditions, precipitation and the SAR wavelength, weighted averages of AGBD from each of the backscatter images are used to obtain a single yearly AGBD estimate. The map is publicly available in the CCI Open Data Portal and hereafter referred to as CCI AGBD.

The EO datasets were not modified or resampled prior to model fitting. For each NFI plot of 56.42 m radius, the mean value of map cells that intersect the plot, weighted by the fraction of the cell that is covered, was estimated. These values are used as covariates at each NFI plot location in the subsequent geostatistical model. The 'exactextractr' package in 'R' is used for this step, and further details are provided in the open-source scripts (see code availability section).

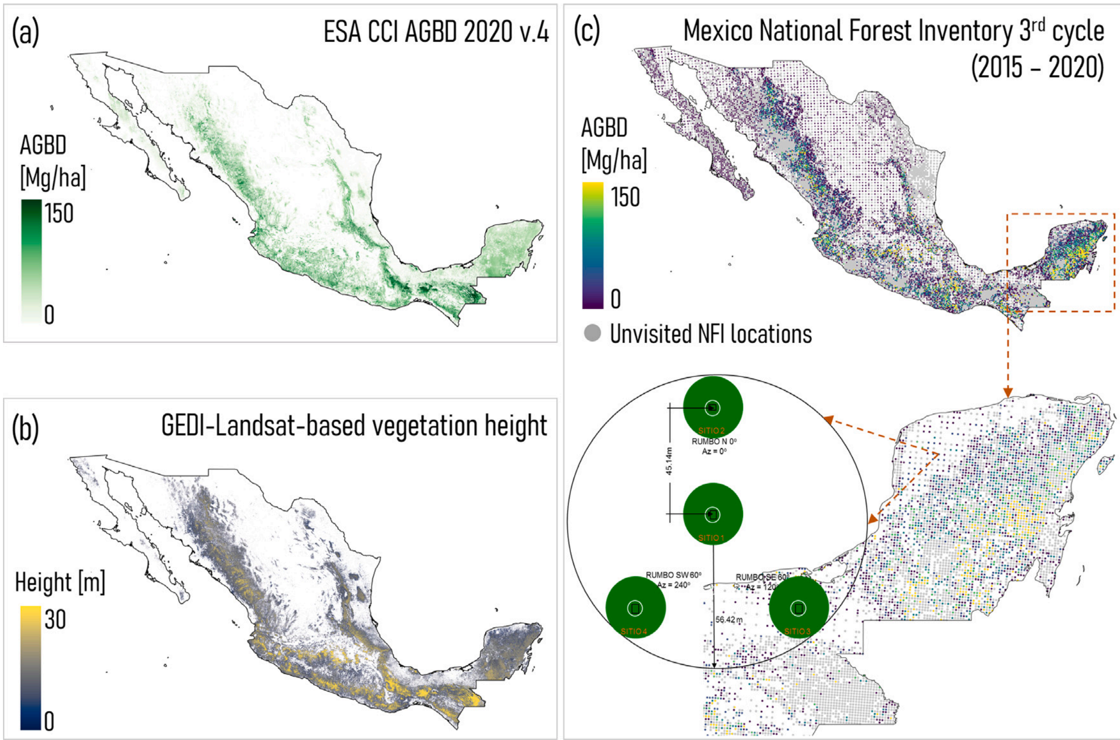

Fig. 1. Sources of the covariates and observations used in the geostatistical model, including the (a) ESA CCI Biomass map, (b) GEDI-Landsat-based height estimates and (c) NFI-estimated AGBD over Mexico (unvisited plots in Mexico's 3rd NFI cycle between 2015 and 2019 are marked in gray).

2.2. Geostatistical modeling of aboveground biomass

To predict AGBD, we implement a geostatistical model-based (GMB) approach with inference conducted through Bayesian methods. In Bayesian approaches, all model parameters and effects are treated as random variables. *Prior* beliefs (in the form of probability distributions) are assigned to these model unknowns, and upon model fitting, these priors are updated with the observed data to produce *posterior* distributions for the model unknowns. We elaborate the GMB approach in the following sections.

A geostatistical model can effectively capture a spatially continuous phenomenon (here, AGBD) that has been observed only at a finite number of sites (visited NFI locations). In essence, many geostatistical models are simply linear regression models with the introduction of spatial effects to account for (1) spatial variation in the residuals and/or (2) spatial variation in the regression coefficients. We assume the model

$$y(s) = \left(\alpha + \tilde{\alpha}(s)\right) + \left(\beta + \tilde{\beta}(s)\right)x_1(s) + \left(\eta + \tilde{\eta}(s)\right)x_2(s) + \epsilon(s), \tag{1}$$

where $y(s)$ is NFI-estimated AGBD, and $x_1(s)$ and $x_2(s)$ are the EO-based covariates at each location s of the NFI plots. The fixed regression parameters are α (an intercept), β and η. Notice that these parameters are not indexed by location s, and are assumed constant across the study domain. However, it is often inappropriate to assume spatially-static forestry models, as covariate relationships and residual errors can exhibit strong spatial patterns (Johnson et al., 2014; May et al., 2023). Therefore, α, β and η are given associated spatial effects $\tilde{\alpha}(s)$, $\tilde{\beta}(s)$ and $\tilde{\eta}(s)$, intended to capture the spatial variation in their respective parameters. This variation is inferred from the observed data during model training. Finally, $\epsilon(s)$ is a normally distributed random error term with mean zero and constant variance σ^2_{ϵ}. While the value of $\epsilon(s)$ changes with location, its variation is assumed spatially independent.

The spatial effects are assumed to follow mean-zero *Gaussian processes* (Gelfand and Schliep, 2016). Taking $\tilde{\alpha}(s)$ for example, for any collection of n locations, $s_1, \ldots, s_n$, the variables at these locations, $\tilde{\alpha}(s_1), \ldots, \tilde{\alpha}(s_n)$, follow a multivariate normal distribution with mean $\mathbf{0}$ and an $n \times n$ covariance matrix. This covariance matrix is generated by a covariance function, $C_\alpha(s_i, s_j)$, providing the covariance between two locations given their relative position. Such covariance functions are typically decaying, meaning that locations close to each other will have large covariance and distant locations will have small covariance between them. The rate of this decay is determined by unknown parameter(s), which must be inferred from the data. We used the popular and flexible Matérn family of functions (Matérn, 1960), that defines the covariance between two points to decay near-exponentially as the distance between them increases (see Appendix).

Spatial effects, and the Gaussian processes that describe them, are not simply a burden that must be surmounted; they are a powerful tool that can aid prediction at unobserved locations. Given a desired prediction location, we can leverage the spatial covariance between this location and the locations of the observed NFI plots to infer values of the spatial effects. Compare this to a non-spatial regression model, where only the covariate values are available at prediction locations. Instead, we infer spatial adjustments that can substantially improve predictive accuracy. The Achilles heel of modeling spatial processes, however, is the computational complexity for large sample sizes due to the resulting large sizes of the covariance matrices. To circumvent the computational burden, we use an approximation approach, the Finite Element Method (FEM) (Zienkiewicz et al., 2005; Lindgren et al., 2011; Rao, 2017). In simple terms, we partition the area of our domain into a finite set of very small areas. As such, a continuous surface across Mexico is instead modeled as a piece-wise linear surface. If the partitioning is fine enough, this piece-wise surface will be indistinguishable from the continuous surface; full details of the FEM are provided in Supplementary Methods.

Our analysis is run in 'R' with package 'R-INLA' (R Core Team, 2022; Lindgren and Rue, 2015), which contains functions to execute efficient geostatistical model fitting and the prediction of AGBD (Gómez Rubio, 2020, Chapter 7). The source code, with detailed explanatory notes intended to ease operational use, is available open-source (see section code availability).

2.3. Bayesian inference and predictions of AGBD

The core output of Bayesian inference is the *posterior* distribution, depicting knowledge of unknown quantities given the observed data. Posterior distributions can be computed for the model parameters as well as for process variables (here, AGBD) at unobserved locations. From these distributions, summaries such as means, standard deviations (SDs) and 95% credible intervals (CIs) can be computed. In this section, we describe the general Bayesian approach, building up to a simpler numerical approach for the prediction of AGBD at any unvisited NFI plot location or any arbitrary area in Mexico.

Let $\mathcal{D}$ be the collection of observed data (NFI-estimated AGBD, plots' geographic locations, covariate values), and $\boldsymbol{\theta}$ be the vector of unknown model parameters/effects and $\pi(\boldsymbol{\theta})$ be the prior distributions for these unknowns. The posterior distribution for $\boldsymbol{\theta}$ is

$$p(\boldsymbol{\theta}|\mathcal{D}) \propto f(\mathcal{D}|\boldsymbol{\theta}) \cdot \pi(\boldsymbol{\theta}). \tag{2}$$

The left side of the equation should be read as "the posterior distribution, $p(\cdot)$, of the parameters given the observed data, $\boldsymbol{\theta}|\mathcal{D}$". This posterior is proportional to, $\propto$, the likelihood function, $f(\mathcal{D}|\boldsymbol{\theta})$, which is determined by our model (Eq. (1)), multiplied by our prior beliefs, $\pi(\boldsymbol{\theta})$. For a desired prediction location s_*, the posterior distribution for AGBD is

$$p\left(y(s_*)|\mathcal{D}\right) = \int f\left(y(s_*)|\boldsymbol{\theta}\right) \cdot p(\boldsymbol{\theta}|\mathcal{D})\, d\boldsymbol{\theta}, \tag{3}$$

which is our model prediction of AGBD, $f\left(y(s_*)|\boldsymbol{\theta}\right)$, integrated across all posterior-plausible parameter values. If there is great uncertainty in the parameter values, this integral will cause larger dispersion and uncertainty in the posterior distribution of $y(s_*)$. Often, predictions are not desired for a particular location, $y(s_*)$ but for an area average, $y(A)$. The posterior for this area average can be computed as

$$p\left(y(A)|\mathcal{D}\right) = \frac{1}{|A|} \int_{s_* \in A} p\left(y(s_*)|\mathcal{D}\right)\, ds_*, \tag{4}$$

integrating all point-wise predictions within the area into an area-wise prediction.

For all but the simplest models, the integrals in Eqs. (3) and (4) are intractable to direct computation. Rather, we generate many random *posterior samples* of $\boldsymbol{\theta}$ from Eq. (2), and then compute Eqs. (3) and (4) using numerical methods. The results converge to the true integral values as the number of posterior samples goes to infinity. In practice, only enough samples are generated to make the resulting numerical errors negligible.

We elaborate the numerical methods to prediction in Eqs. (6)–(10). The method are also summarized in Fig. 2, with the view of it serving as an intuitively comprehensible and executable approach that may be used in policy-related reports.

2.3.1. Prediction at a single unvisited location

Let s_* represent a desired prediction location, where properties of the posterior distribution, $p\left(y(s_*)|\mathcal{D}\right)$, must be approximated numerically. To do so, $m = 1, \ldots, M$ random samples are drawn from the posterior distribution of $\boldsymbol{\theta}$ (Eq. (2)). Samples from the pertinent parameters/effects are then plugged in to the model (Eq. (1)) to yield random posterior samples for AGBD, $y(s_*)$, at the location s_*:

$$y_{(m)}(s_*) = \left(\alpha_{(m)} + \tilde{\alpha}_{(m)}(s_*)\right) + \left(\beta_{(m)} + \tilde{\beta}_{(m)}(s_*)\right) x_1(s_*) + \left(\eta_{(m)} + \tilde{\eta}_{(m)}(s_*)\right) x_2(s_*) + \epsilon_{(m)}(s_*). \tag{5}$$

Properties of the posterior distribution, such as the expected mean value, $\overline{y}(s_*)$, and SD, $\sigma(s_*)$, of AGBD, can then be approximated with the corresponding sample quantities,

$$\mathrm{E}\left[y(s_*)|\mathcal{D}\right] \approx \overline{y}(s_*) = \frac{1}{M} \sum_{m=1}^{M} y_{(m)}(s_*), \tag{6}$$

$$\mathrm{SD}\left[y(s_*)|\mathcal{D}\right] \approx \sigma(s_*) = \sqrt{\frac{1}{M-1} \sum_{m=1}^{M} (y_{(m)}(s_*) - \overline{y}(s_*))^2}\ . \tag{7}$$

By the law of large numbers, the approximations become exact as $M \to \infty$. In practice, since one cannot generate infinite posterior samples, we settle to generate enough to make the approximation error negligible. A rule of thumb for a sufficient number of samples is difficult to prescribe, as it varies by scenario. However, stability of the sample quantities (e.g., Eqs. (6) and (7)) can be assessed using trace plots: cumulatively computing the quantities for increasing M until an apparent asymptote has been reached.

2.3.2. Predictions over an arbitrary area

Over any arbitrary geographic area larger than the size of a single NFI plot, inference of area-wide mean AGBD and its associated uncertainty involves analyses of posterior predictions at multiple locations within the area. Assume the desired area, A, can be partitioned into a grid of N hypothetical NFI plots at locations $s_{1,*}, \ldots, s_{N,*}$. The area AGBD, $y_{(m)}(A)$, is then

$$y_{(m)}(A) = \frac{1}{N} \sum_{i=1}^{N} y_{(m)}(s_{i,*}). \tag{8}$$

As $m = 1, \ldots, M$ random samples are drawn from the posterior distribution of $\boldsymbol{\theta}$ (Eq. (2)), the mean area-wide AGBD, $\overline{y}(A)$, and standard deviation, $\sigma(A)$, is:

$$\overline{y}(A) = \frac{1}{M} \sum_{m=1}^{M} \overline{y}_{(m)}(A), \tag{9}$$

$$\sigma(A) = \sqrt{\frac{1}{M-1} \sum_{m=1}^{M} (\overline{y}_{(m)}(A) - \overline{y}(A))^2}\ . \tag{10}$$

For computational convenience, the predictive grid of hypothetical NFI plots may not need to be as dense as a "wall-to-wall" plot partition, and a coarser grid may suffice. For example, to predict over a 10,000 km^2 area, the results of a 1 km grid and a 100 m grid would likely be indistinguishable. A sufficient density of the grid to predict the area AGBD may be tested by comparing the relative improvement in the precision of the mean area-wide AGBD estimations with increasing grid density.

2.4. Model validation

To validate the model, we first gauge the appropriateness of the shape of the posterior predictive distributions using a leave-one-out cross-validation during the process of model fitting. A cross-validated Probability Integral Transform (PIT) is generated, which assesses, for each observation, the probability that the posterior mean prediction will be less than or equal to the observed value (David and Johnson, 1948).

$$\mathrm{PIT}_i = \mathrm{Prob}(y_i^{pred} \leq y_i^{obs}|y_{-i}), \tag{11}$$

where y_i^{pred} is the prediction where y_i^{obs} is the observed value, and y_{-i} denotes the observations with the ith observation omitted. When the model accurately represents the observations, the PIT scores are expected to be uniformly distributed between 0 and 1. The estimation of PIT is inbuilt within the package 'R-INLA', providing an assessment of the accuracy of the calibration of out-of-sample predictions during model training (Held et al., 2010; Gómez Rubio, 2020).

Since the overall objective of the study is to enable location-specific and area-wide prediction of AGBD with reliable inference and uncertainty, a second cross-validatory check is performed by holding out a random test sample of 10% of observations from the model fitting. Predicting mean AGBD and its posterior distribution on the withheld set provides an indication of the model performance at unobserved

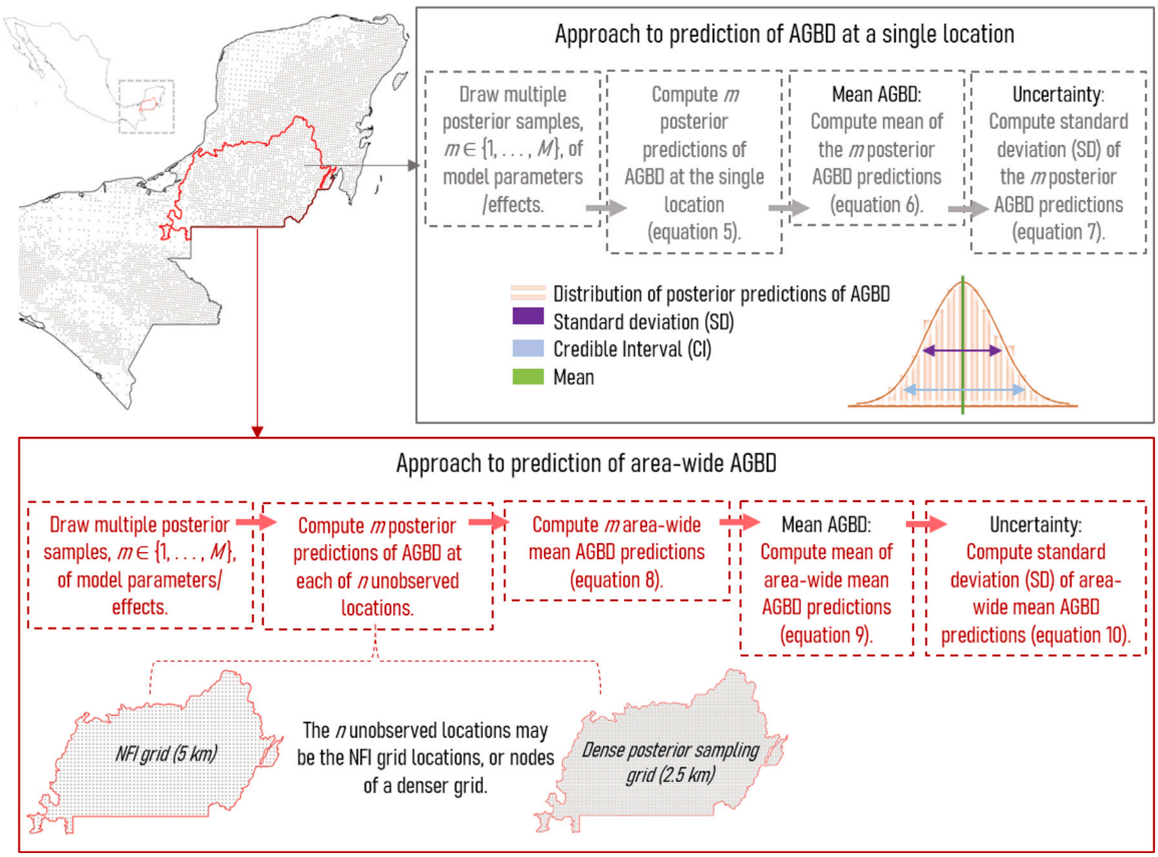

Fig. 2. Numerical approach to Bayesian inference and posterior prediction of mean AGBD at either a single location or across an arbitrary area (e.g. the stratum displayed in red, "Lomerios of the South of Yucatan peninsula with high and medium sub-evergreen forest"). For the area-wide AGBD, a predictive grid, with a maximum density of hypothetical "wall-to-wall" NFI plots, is used.

locations. To gauge the accuracy of the posterior expected values in comparison to the test values, an R-squared metric and root mean squared error (RMSE) serve as heuristics,

$$\tilde{R}^2 = 1 - \frac{\sum_{i=1}^{t_*} \left(E[y(s_{*,i})] - y(s_{*,i}) \right)^2}{\sum_{i=1}^{t_*} \left(y(s_{*,i}) - \bar{y}_* \right)^2} \tag{12}$$

$$\text{RMSE} = \sqrt{\frac{\sum_{i=1}^{t_*} \left(E[y(s_{*,i})] - y(s_{*,i}) \right)^2}{t_*}} \tag{13}$$

where $s_{*,i};\ i \in \{1, \ldots, t_*\}$ are the test locations with observed values of $y(s_{*,i})$, $\bar{y}_*$ is the mean of those observed values, and $E[y(s_{*,i})]$ are posterior mean predictions at the test locations.

3. Results

3.1. Geostatistical model results

Prior to presenting predictions of AGBD, we discuss a few intermediate results that were relevant to the process of model training. First, the two covariates (CCI AGBD and GEDI-based height estimates), individually, were moderately correlated to NFI-estimated AGBD. A square root transformation of the response variable was applied to linearize the relationship (Fig. 3). In this section, each posterior prediction of the response variable (in units $(\text{Mg/ha})^{1/2}$) is back-transformed to the original scale (units Mg/ha) where necessary. Second, in Bayesian approaches, prior distributions of model parameters can be made informative (potentially influential on the modeling results) or non-informative, depending on the availability of defensible prior beliefs. Prior specifications often become irrelevant as the sample size grows large, as the posterior distribution becomes dominated by the data likelihood ($f(\mathcal{D}|\boldsymbol{\theta})$ in Eq. (2)). We tested weakly informative priors on spatially-varying random effects (e.g. probability that the range of covariance is less than 30 km is 0.01), and found negligible influence on AGBD predictions, implying that our results were driven primarily with information from the data and not on prior beliefs.

Summaries of the posterior distributions of both sets of model parameters, fixed effects and spatially-varying random effects, are displayed in Fig. 4a and 4b, respectively. The components of fixed effects explained 62% of the variance in the observed AGBD (square-root transformed values), the spatially-varying effects explained another 19%, while the remained is expected to be captured by the random error (ϵ, Eq. (1)). The spatially varying random effects ($\tilde{\alpha}$, $\tilde{\beta}$ and $\tilde{\eta}$) are best understood by visualizing their spatial structure and decay of covariance with distance. Take $\tilde{\alpha}$ (intercept), which explained 8.32% of the variance in the response variable, as an example: posterior means were largest in ecoregions of the Sierra Madre Occidental mountain ranges, smallest in the arid deserts of northern/central Mexico, and the covariance was predicted to decay to <0.05 $(\text{Mg/ha})^2$ at ~400 km (Fig. 4b, left column). The results inform on importance of accounting for spatial variation in model parameters to appropriately glean information from the EO datasets for AGBD prediction. The leave-one-out cross-validation resulted in a fairly uniform distribution of PITs, implying that the posterior samples of predicted AGBD (here, square-root transformed values) do not have a larger probability of being over- or under-predictions when compared to their observed values (Fig. 5a).

Next, the model's performance on the withheld 10% of observations was examined. As is common in Bayesian inference, 1000 samples of model parameters were drawn from their posterior distributions, and 1000 posterior predictions of (square-root of) AGBD were subsequently generated for every withheld NFI location (note that

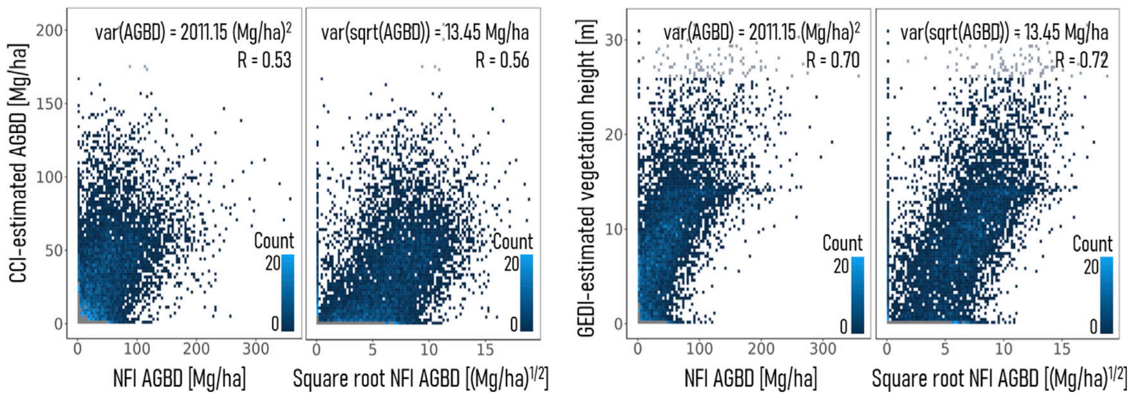

Fig. 3. Observations (NFI-estimated AGBD) in original scale and square-root transformed scale, plotted against vegetation AGBD and height estimated from EO datasets. The variance of the observations and the Pearson's correlation coefficient (R) is displayed.

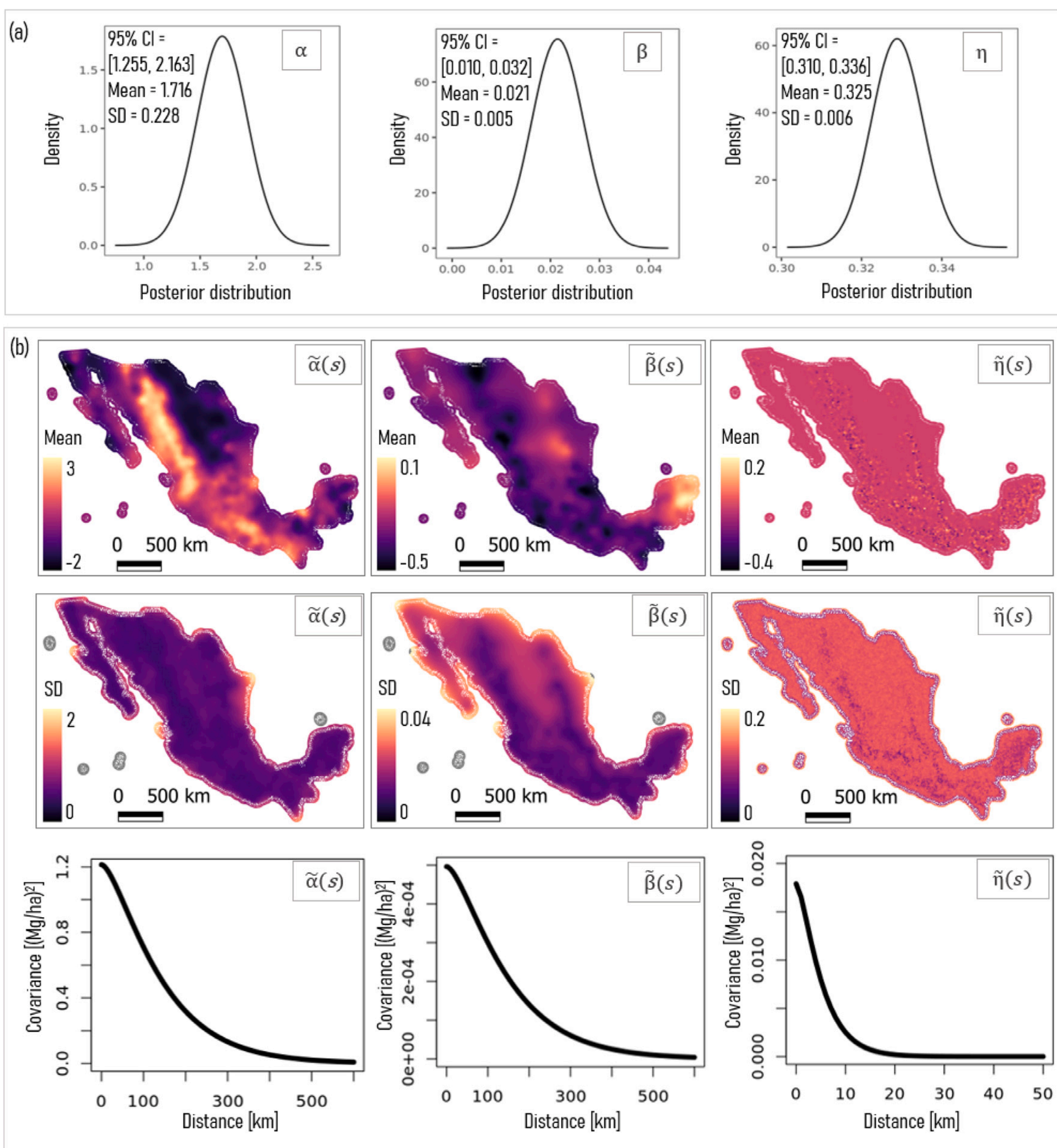

Fig. 4. Geostatistical model (Eq. (1)) results. (a) Posterior distributions of the fixed-effects parameters (α, β and η), including means, standard deviations (SDs) and 95% credible intervals (CIs). (b) Posterior mean and SDs of the spatially-varying random effects ($\tilde{\alpha}(s)$, $\tilde{\beta}(s)$ and $\tilde{\eta}(s)$) across Mexico, and their covariance as a function of distance.

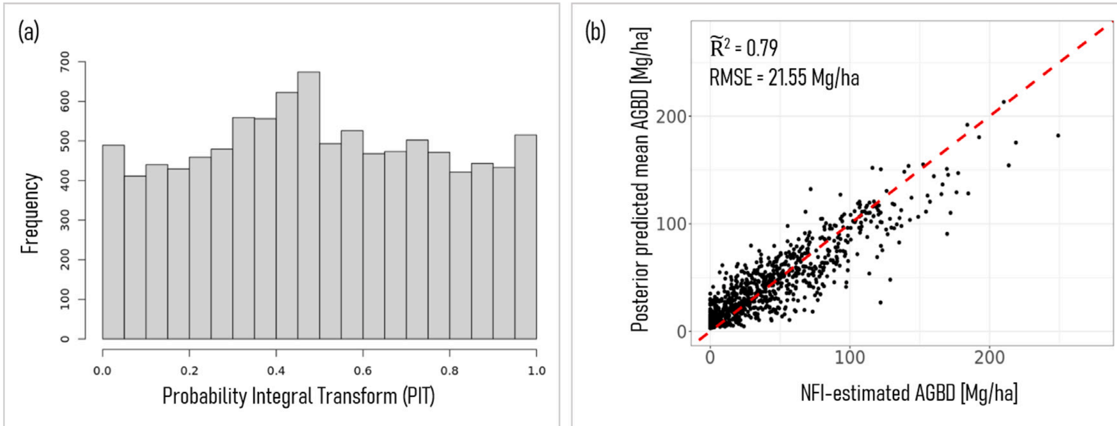

Fig. 5. Results of cross-validation of model showing (a) histogram of probability integral transform (PIT) and (b) posterior mean predictions of AGBD in the withheld cross-validation sample of 10% of NFI plots, plotted against their observed values.

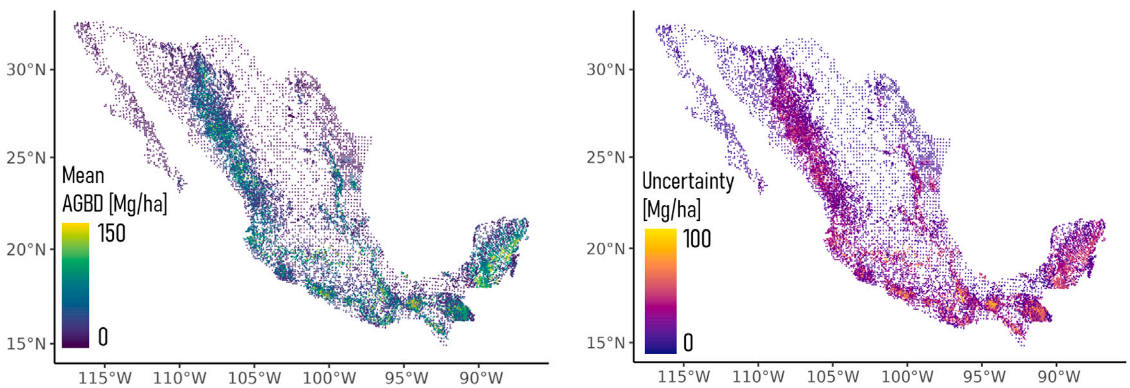

Fig. 6. Posterior mean predictions of AGBD and associated uncertainty (i.e. standard deviation (SD) of mean predictions) at unvisited locations in the 3rd NFI cycle.

increasing the number of samples had negligible impact on results). Upon back-transforming posterior samples (square-root of AGBD and to its original scale), for each location, the full posterior distributions of AGBD predictions was available. Summaries, such as the mean of these 1000 predictions, their 2.5% and 97.5% quantiles (95% CI) and their standard deviation (SD, uncertainty on the mean) were calculated (Eqs. (6)–(7)). A difference of means between NFI-estimated AGBD and GMB-predicted AGBD of 0.30 Mg/ha was found, with an $\tilde{R}^2$ of 0.79 and RMSE of 21.55 Mg/ha (Eqs. (12)–(13)), providing evidence of fairly accurate posterior predictions compared to the test values.

The posterior predictions of the withheld observations indicate some evidence of systematic under-prediction in higher ranges of AGBD (e.g. AGBD > 100 Mg/ha, Fig. 5b). Since the full posterior distributions of AGBD predictions at each location were available, we tested the coverage rate of the 95% credible intervals (CIs), i.e. the proportion of withheld NFI locations and their AGBD estimates lying within the 95% CIs of our model AGBD predictions. The coverage rate will ideally be 95%; coverage rates below 95% indicate that model uncertainties may be overly optimistic, while rates above 95% suggest that uncertainties could be overly conservative (see May et al., 2023). Our model returned an appropriate coverage rate of 96%, providing evidence of reliable uncertainty estimates of AGBD predictions overall. For locations with AGBD observations > 100 Mg/ha, the coverage reduced to 92% as more observations (i.e. NFI-estimated AGBD) were above the upper bound of the credible intervals of the predictions. For these locations, a difference in means of ~28 Mg/ha was found, indicating the 95% CIs may be too narrow and overly optimistic. Possible reasons for the observation of some systematic under-prediction at the higher end of AGBD ranges are discussed in Section 4. For locations with AGBD observations ≤100 Mg/ha, an appropriate coverage rate and a difference in means of ~3 Mg/ha is noted.

3.2. Operational use of model

The details of operational use are detailed in the sections that follow.

3.3. Predictions over non-vegetated areas

Our model (Eq. (1)) assumes that a part of the residuals can be explained by smooth spatial variations across the domain, and the remainder by a random error, ignoring vegetated and non-vegetated land boundaries. Some of these boundaries are inbuilt in our datasets. The GEDI-based vegetation height estimates use a number of empirical thresholds, including only woody vegetation heights of ≥3 m, an urban and water mask, and optical indices, slope and elevation thresholds (Potapov et al., 2021). Similarly, the CCI biomass map includes masks urban areas, snow and ice, and water bodies (Santoro et al., 2024). Where surveyed, NFI plots located in agricultural or urban areas with no natural vegetation are recorded with AGBD of 0 Mg/ha. Hence, our observations and covariates inherently contain discrete land boundaries, at which near-zero AGBD will be predicted in the ideal scenario. In presenting the operational use of the model for predictions in the sections that follow, and in the source code (see section code availability), we allow for the (optional) use of a national urban areas mask (INEGI, 2020) and likelihood of forest cover layer (Braden et al.,

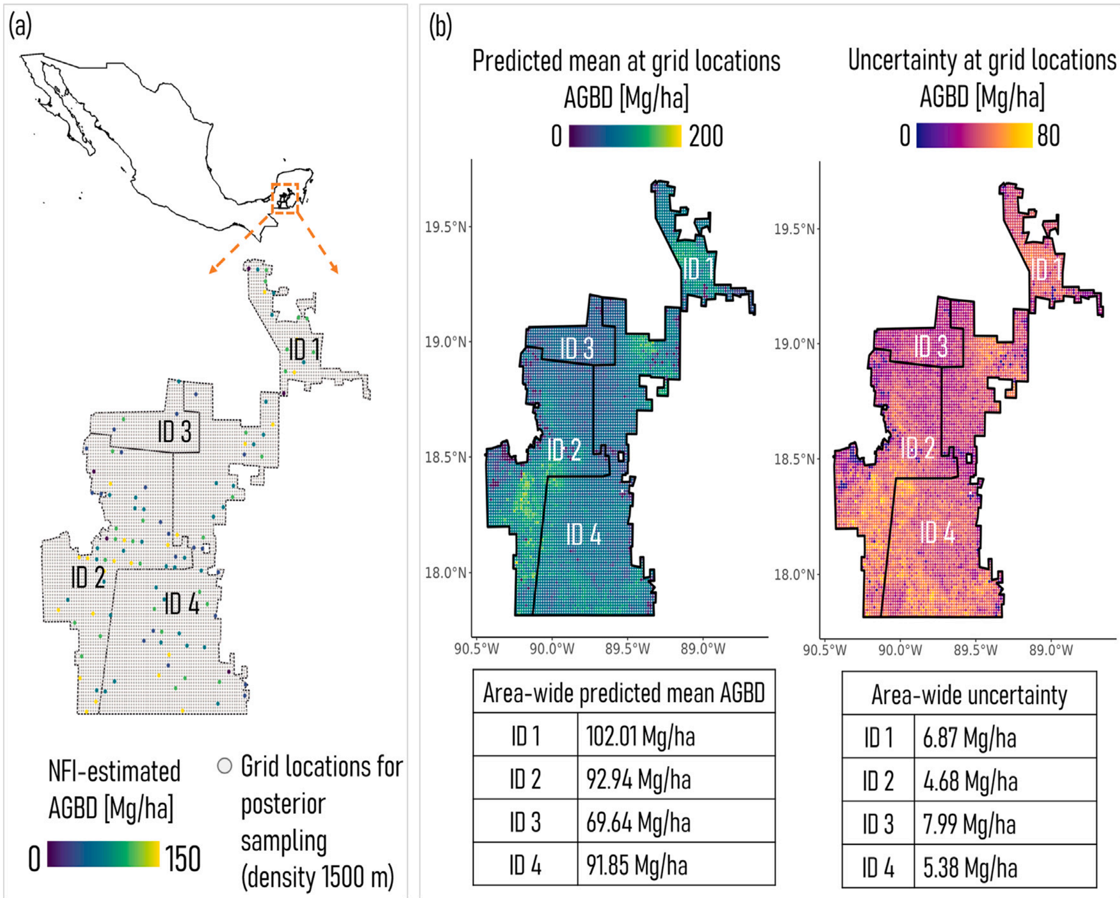

Fig. 7. (a) Natural Protected Areas (NPAs, IDs 1–4) in evergreen forests of the south Yucatan peninsula, with NFI-estimated AGBD at a sparse set of locations. A grid of point density 1500 m is generated in each NPA for prediction of AGBD with the geostatistical model (eq (1)). (b) Posterior predicted mean and standard deviation (SD) at each location of the grid (Eqs. (6)–(7)), with tables summarizing the area-wide mean AGBD and associated uncertainty (i.e. SDs of area-wide mean predictions) for each protected area (Eqs. (9)–(10)).

2024), such that posterior predictions are restricted to only vegetated areas. Further, given the formulation of our model, predictions of square-root transformed AGBD ≤ 0 $(\mathrm{Mg/ha})^{1/2}$ were entirely possible. The count of predictions of below 0 were noted, reported, and fixed to equal 0.

3.3.1. Location-specific predictions

The first application of the GMB results is the prediction of AGBD in the 15,261 unvisited 3rd-cycle NFI locations, (with no vegetated-area mask applied). Similar to the test observations, 1000 samples of model parameters were drawn and 1000 posterior predictions of AGBD subsequently generated for every unvisited NFI location (Eqs. (6)–(7), with results in Fig. 6). As in the visited locations of the NFI, the predicted range of AGBD was up to 390 Mg/ha, with the largest values in the tropical humid forests of southern Yucatan peninsula. The smallest ranges of AGBD were, as expected, observed in the arid deserts of northern/central Mexico. Overall, only 0.4% of locations resulted in a posterior mean predictions of below 0 $(\mathrm{Mg/ha})^{1/2}$, and were set to equal 0 before back-transforming to original scale of AGBD.

3.3.2. Area-wide predictions

The second demonstrated application of the GMB is the area-wide assessment of AGBD in regions that have been under-sampled in the NFI due to accessibility and logistic constraints. Four Natural Protected Areas (NPAs) (CONABIO CONANP, 2024) of the southern Yucatan peninsula (Selva Maya region, with extensive tropical rainforests), within which 131 irregularly-distributed NFI plots were visited in the 3rd-cycle of the NFI, were chosen to exemplify posterior AGBD predictions (Fig. 7a). A dense grid of spacing of 1500 m was created to analyze the NPAs, excluding delineated urban and rural built-up areas (INEGI, 2020) within. Computed posterior distributions of AGBD captured at each grid node across the NPAs, and their area-wide summary statistics (using Eqs. (9)–(10)), are provided in Fig. 7b. The relative uncertainty of area-wide AGBD predictions (ratio of posterior SD to posterior mean) in these NPAs was below 15% (below 8 Mg/ha in absolute values), indicating that model provides highly precise posterior predictions of mean area-wide AGBD.

For the remainder of terrestrial NPA's across Mexico (excluding lakes, lagoons, marine islands and beaches), posterior predictions of mean and SD of AGBD are provided in Fig. 8 and Supplementary Material, File 1. For each of these NPAs, the absolute uncertainty of area-wide mean AGBD predictions was below 30 Mg/ha. For over one third of these NPAs, this corresponded to a relative uncertainty of <30%. Protected areas with sparse vegetation and low ranges of biomass, such as those in arid lands or in close proximity to urban/rural areas, exhibited amongst the largest relative uncertainty.

A further example of the use of the model is the predictions of AGBD in the 186,241 community forest management and payment for environmental services projects supported by CONAFOR across Mexico. These project areas range from 2 ha to 552,569 ha in size, with the

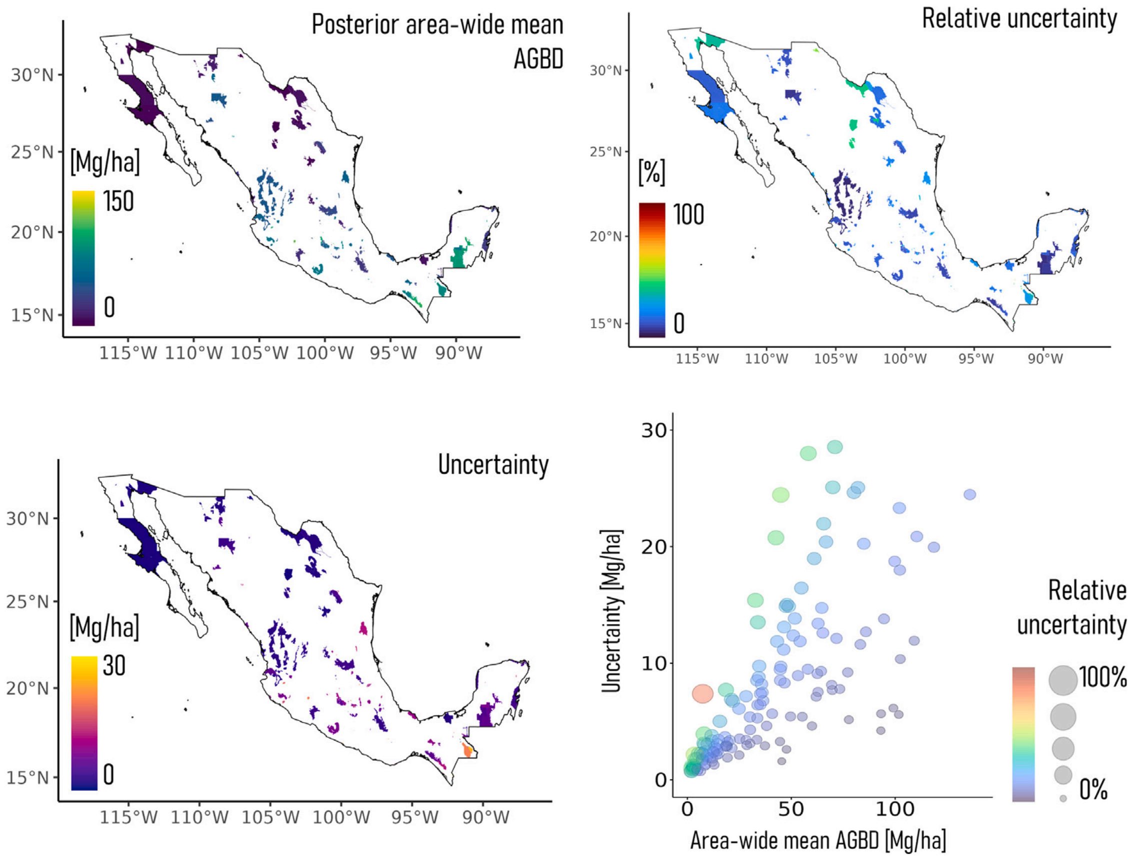

Fig. 8. Posterior predictions of area-wide mean and its uncertainty in all terrestrial Natural Protected Areas (NPAs) in Mexico. Relative uncertainty is the ratio of posterior standard deviation (SD) to posterior mean. Scatter plot shows the relative uncertainty, with each point representing an NPA.

smaller projects rarely overlapping any NFI plots of the 3rd cycle. For each project area, posterior predictions of AGBD were computed at locations of hypothetical wall-to-wall NFI plots placed in a grid, i.e. 100 m × 100 m (Fig. 9). The wealth of information provided by summary statistics of the posterior distributions at each grid node is exemplified for one project area in Fig. 9.

3.3.3. Predictions in broad terrestrial ecological strata

Predicting AGBD across any arbitrary area with our model, in the ideal scenario, relies on a dense sampling grid at which posterior predictions are generated, e.g. wall-to-wall hypothetical NFI plots. However, across very large areas (> 1 Mha, for example), the computational burden of posterior sampling in dense grids may not necessarily correspond to a gain in precision of area-wide AGBD predictions. For example, for the four Natural Protected Areas (NPAs) exemplified in Section 3.3.2, a grid density of 1500 m was sufficient to capture precise mean area-wide mean AGBD estimates. For the broad terrestrial ecological strata of Mexico (level 1), which are commonly used delineations for policy reports, we next demonstrate the use of our model while testing varying grid densities to assess the impact on the precision of area-wide mean AGBD predictions.

The ecological strata are available at different levels; the coarsest classification is seven broad ecological zones for the country, and the finest is 101 strata with different ecosystem characteristics and vegetation types (download available at CONABIO, 2008). For the finest level, the density of the sampling grid to predict AGBD was adjusted incrementally from points spaced 20 km to 500 m apart. Urban and non-forest areas (using INEGI (2020) and Braden et al. (2024)) with the strata were excluded, with the flexibility to adjust definitions of these delineations in the source code (see section code availability). Results indicated that for nearly all ecological strata, mean area-wide predicted AGBDs change negligibly with increments in grid density (Fig. 10a, left), but gains in precision were found at least up to grid densities of 5 km, after which an asymptote is typically reached (Fig. 10a, right). Stratum-wise posterior predictions at a grid density of 500 m are displayed in Fig. 10b. For coarser levels of stratified ecoregions commonly used in policy reports, sampling at grid densities of 5 km was considered sufficient, and posterior predictions of AGBD are provided in Supplementary Material, Table 1.

4. Discussion

To date, there has been limited progress in the formal adoption of global EO-based datasets in (sub)national monitoring and reporting of biomass stocks. In this study, we present a geostatistical model-based approach to enhance Mexico's 3rd NFI sampling cycle, gap-fill unvisited NFI locations and predict AGBD across any spatial extent, leveraging the strengths of some of the newest global EO datasets as of 2024 - GEDI-based vegetation height and the 2020 CCI AGBD estimates.

Geostatistical models that incorporate spatially varying components to capture non-stationary relationships between covariates and the response variable have practical underpinnings in various fields of science (Cressie, 2015). Further, our inference is based on well established principles of Bayesian statistics. From a methodological perspective, the contribution of this study does not lie solely in the presented approach. Instead, the contribution of the study is the co-development of an operationally-feasible approach with CONAFOR in Mexico, and the public release of source code for the direct and transparent generation of estimates that may be used in climate policy reporting. This code is provided with the flexibility to incorporate vegetation masks (e.g. urban or (non)forest areas) and to be executable from project-level scales to the broad regional to national scales of Mexico. It provides a

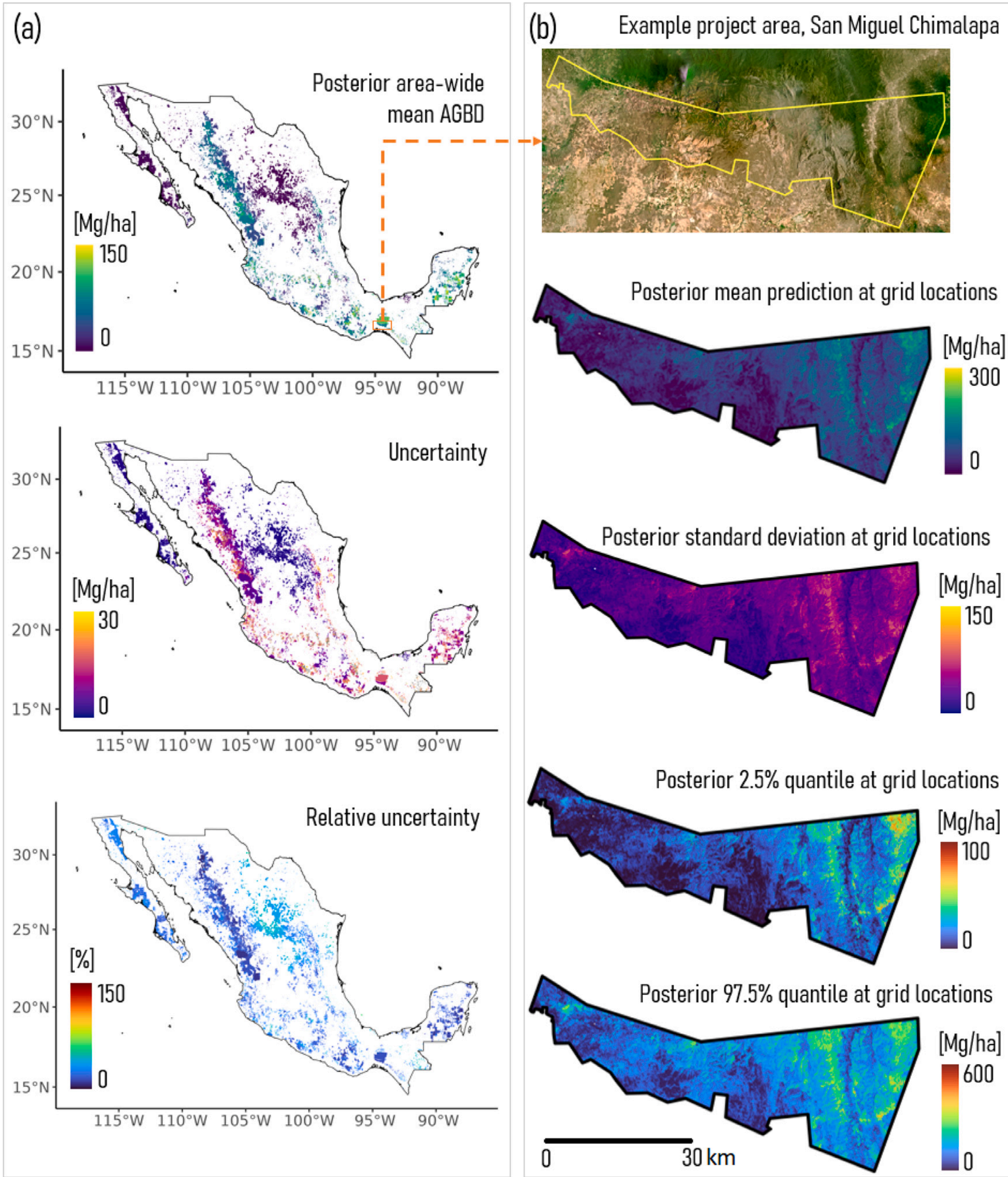

Fig. 9. (a) Posterior predictions of area-wide mean and uncertainty in community forest management and payment for environmental services projects in Mexico. Relative uncertainty is ratio of posterior standard deviation (SD) to posterior mean, for each of the 186,241 projects. (b) For a selected project site in Oaxaca in south-western Mexico, the posterior distribution of predictions of AGBD at each grid node (100 m × 100 m) are exemplified.

coherent and intuitively-comprehensible framework to propagate the uncertainty in model parameters to single-location and area-wide predictions of AGBD. This level of transparency and clarity is particularly advantageous for climate change mitigation initiatives that mandate auditing of technical analysis and related reports. The model-fitting in 'R' statistical software on a 32-GB or 64-GB RAM machine is achieved within 60-120 min, while the processing time required for predictions range from a few minutes to hours depending on the complexity of the area(s) of interest. Hence, the approach is considered computationally viable, resulting in vegetation AGBD estimates with traceable sources of uncertainty. Note, this finding must not be misinterpreted as the ability to entirely replace NFIs with global-scale EO datasets; modeling the latter with the former, as in this study, is a means for rigorously scaling NFIs and thereby obtaining AGBD predictions at single locations or over arbitrary areas.

Overall, the proposed geostatistical model shows strong performance using the chosen EO-derived datasets as covariates, evidenced by the large R-squared and small RMSE heuristics (0.79 and 21.55 Mg/ha respectively) for predictions of AGBD in withheld validation locations. Notwithstanding, if the method is to be applied in nations other than Mexico, certain considerations, challenges and recommendations for improvement must be addressed. For example, although not dependent on a probability sample of field observations, the model does rely on a fairly balanced representation of vegetation types and AGBD ranges in the field observations across Mexico. If the intention is the prediction of AGBD in all ecological strata of a country, NFI plot observations are desirable in regions ranging from low-AGBD

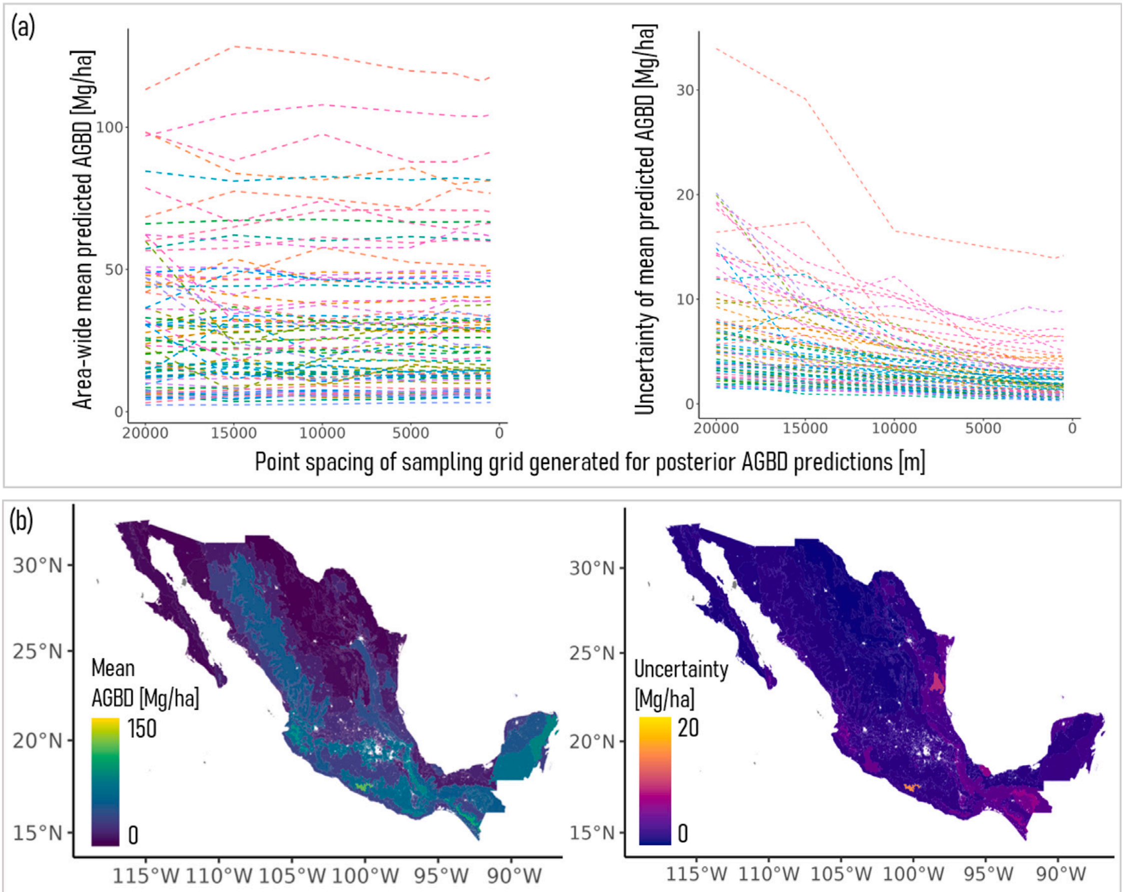

Fig. 10. (a) Area-wide mean predicted AGBD (left) and associated uncertainty (i.e. standard deviation (SD) of mean predictions, right) in terrestrial ecological stratum of Mexico (each colored dashed line represents a single stratum). These summary statistics are obtained from posterior predictions of AGBD at nodes of user-created grids with point spacing ranging from 20 km to 500 m. (b) Resulting maps of mean of stratum-wise AGBD and uncertainty using a 500 m grid density.

(e.g. deserts) to high-AGBD (e.g. rainforests) for model training. Nations that aim to apply similar approaches will require inventories that are representative of AGBD ranges in the regions predictions are needed, and the testing of the validity of the model across their ecoregions. Further, although feasible to incorporate in model training, the absence of any prior information on errors in the NFI-estimated AGBD implies that they cannot not be explicitly defined in the model. This includes training data on geolocation errors, errors in allometric models, errors caused by measuring only four sub-plots in the sample plot and any measurement errors in these sub-plots, all of which would need the use of other methods (such as destructive harvesting) or instruments (such as terrestrial laser scanning) to be appropriately approximated (Réjou-Méchain et al., 2019). The inherent assumption that these errors are either negligible and insignificant, or significant but random and unbiased so they aggregate to near-zero over plots (see McRoberts and Westfall, 2013), remains untested.

Another common challenge in the estimation of biophysical properties of vegetation from EO data is 'saturation', or the decreased sensitivity of signals to changes in these properties, above certain ranges. Although purely GEDI's lidar canopy height estimates will exhibit little to no saturation (see Dubayah et al., 2020; Duncanson et al., 2022), their extrapolation with optical indices may; for example, using a GEDI-Landsat fused product (Potapov et al., 2021) for this study captured heights only up to ~37 m in Mexico's vegetated areas. Similarly, the CCI Biomass maps provide decreasingly informative estimates beyond approximately 150 Mg/ha to 200 Mg/ha (Santoro et al., 2021, 2024). Now, allowing for spatial flexibility in our model parameters, borrowing strength across space and incorporating spatial autocorrelation in our approach, reduces some of the possible effects of saturation in the model fit and prediction of AGBD. However, the slightly lower coverage rate and differences in mean predicted biomass noted in areas of AGBD > 100 Mg/ha in our results (see Section 3.1) may still be related to the poor representation of these areas in the chosen auxiliary covariates.

For nations intending to use EO datasets to enhance forest inventories, considerations of saturation are important because they may potentially lower model accuracy. How may this be avoided? By design, the GEDI instrument samples discretely along orbital transects, and since the probability of collocation with plots of NFIs is small, complete-coverage estimates of vegetation height to achieve overlap with NFI plots may continue to rely on multi-sensor data fusion. If preference is given to using GEDI data in combination with datasets that are less subject to saturation, model accuracy may be retained even at high AGBD ranges. Alternately, newer methods have demonstrated the generation of probabilistic GEDI waveform predictions over NFI plots locations (May et al., 2024), overcoming the need to have collocated GEDI-plot observations and thereby negating the need for multi-sensor data integration. Although these methods remain to be tested, the reliance on either solely gridded GEDI vegetation height estimates, and/or imputed GEDI waveforms for height estimates at desired locations, may avoid limitations caused by saturation. For SAR-based covariates, such as the CCI Biomass map, a move to estimating AGBD with long-wavelength radar (e.g. P-band from the upcoming

BIOMASS mission) may be the only viable option to reduce the effects of saturation in regions of high biomass (Quegan et al., 2019). Importantly, irrespective of the chosen input covariate, it must be sourced or produced independently of the NFI data. Further, countries must rigorously test the relations of all covariates with NFI-estimated AGBD prior to fitting geostatistical models. It is inadvisable to use the same covariates as in this study without such investigations; for when covariates are EO-derived vegetation heights or biomass maps, whether of global- or national-scale, they must be independent of the NFIs and exhibit meaningful relations to NFI-estimates to result in reliable and accurate AGBD predictions.

A notable drawback of the study in the context of its use in policy-related reporting is that it only provides a method for mono-temporal predictions of AGBD, offering a static view of baseline AGBD in Mexico in approximately 2020. Instead, many policy-related applications can benefit from assessments of AGBD *change* (biomass stock-change or gain-loss estimates (IPCC, 2006, Volume 4, Chapter 2, p. 2.10)). Note that Bayesian spatio-temporal approaches are executable in a similar model-based framework as demonstrated in this study (Gómez Rubio, 2020, see Chapter 8.6), but require multi-temporal inputs of covariates and the response variable, both of which were lacking for this study. This lack of data pertains particularly to the GEDI-based vegetation-height estimates, which explain a large portion of the variance of AGBD in Mexico, but were unavailable prior to 2019. Can this shortcoming be overcome in subsequent research? To do so, a primary requirement would be to ensure the availability of consistent data streams for EO-based covariates (such as space-based lidar from the proposed EDGE mission EDGE, 2024) simultaneously over the period of collecting new NFI data, thereby enabling the development of spatio-temporal models. Countries aiming to adopt EO datasets in biomass assessments with such models must design spatially well-distributed NFI sampling that allows for consistent repeat observations. Moving on from there, international coordination bodies working in planning space missions must strive for the continuity of the same EO data streams in the future; only through such long-term complementarity between NFIs and EO-based covariates can countries regularly and consistently rely on models to generate estimates of biomass.

The number of open source EO datasets specifically aimed at supporting global forest monitoring is expected to increase with the launch of new satellite missions, such as JAXA's Advanced Land Observing Satellite-4 (ALOS-4) (JAXA, 2024), ESA BIOMASS (Quegan et al., 2019) and the NASA-ISRO Synthetic Aperture Radar (NISAR) (NASA-JPL, 2019). For these missions, and any future lidar-based missions, developing open-science approaches to integrate their data with NFIs must remain a scientific priority. The release of new data streams in conjunction with the release of operationally feasible approaches, developed in collaboration with in-country teams, is likely to facilitate their uptake for national climate change mitigation actions. As demonstrated in this study, this will allow countries to take advantage of global-coverage space-based biomass datasets to provide more spatially-detailed regional and national estimates of biomass. If this is desired, countries designing new NFIs must consider geographic representativity and robust sampling approaches, which will permit the ease of integration with incoming EO data streams. In the long run, the success of supporting National Forest Monitoring Systems with EO will strongly depend on in-country institutional will, financial resources and coordination with producers of the EO datasets (Neeff and Piazza, 2019). If supportive policy guidance with which countries may evaluate the need and method with which to integrate model-based results in reporting is released in parallel, EO data will play a greater role in aiding global climate policy requirements.

5. Conclusion

Our study provides a transparent and computationally feasible geostatistical approach to enhancing biomass assessments in Mexico with EO datasets. The approach augments the nation's well-established forest monitoring system, with its outcomes enabling the prediction of biomass in any area of interest – single-location or area-wide spatial scales – with traceable uncertainty analyses. The results fill a gap between national, design-based NFI efforts and the need for more regional- to project-level assessments of biomass. The co-development of the methodology with CONAFOR ensures reciprocal knowledge and technology transfer, addressing Mexico's policy needs and facilitating operational use. It is hence a step to lessen the increasingly widening gap between the fast-growing developments in geospatial research and the country demands for operational systems, integrating processes and institutions involved in policy making (Herold et al., 2019). For nations other than Mexico, challenges in the use of the proposed approach may primarily concern the representativeness of observations (NFI-estimates of AGBD) and covariates (GEDI-based vegetation height and the 2020 CCI AGBD estimates) across their respective ecoregions and biomass ranges. To achieve meaningful results with geostatistical model-based approaches, our study recommends rigorously testing that EO datasets fairly represent vegetation in the ecozones of these nations. The selection of appropriate EO-based covariates, with considerations of minimizing the effects of saturation, will be important to accurately glean information that enhances (sub)national estimates of biomass.

CRediT authorship contribution statement

Neha Hunka: Writing – review & editing, Writing – original draft, Visualization, Project administration, Methodology, Investigation, Formal analysis, Data curation, Conceptualization. **Paul May:** Writing – review & editing, Writing – original draft, Methodology, Investigation, Formal analysis, Data curation, Conceptualization. **Chad Babcock:** Writing – review & editing, Writing – original draft, Methodology, Formal analysis, Conceptualization. **José Armando Alanís de la Rosa:** Writing – review & editing, Writing – original draft, Methodology, Investigation, Formal analysis, Data curation, Conceptualization. **Maria de los Ángeles Soriano-Luna:** Writing – review & editing, Writing – original draft, Methodology, Investigation, Formal analysis, Data curation, Conceptualization. **Rafael Mayorga Saucedo:** Writing – review & editing, Writing – original draft, Methodology, Investigation, Formal analysis, Data curation, Conceptualization. **John Armston:** Writing – review & editing, Writing – original draft, Methodology, Investigation, Data curation, Conceptualization. **Maurizio Santoro:** Writing – review & editing, Writing – original draft, Methodology, Investigation, Formal analysis, Data curation, Conceptualization. **Daniela Requena Suarez:** Writing – review & editing, Writing – original draft, Methodology, Investigation, Formal analysis, Conceptualization. **Martin Herold:** Writing – review & editing, Writing – original draft, Methodology, Investigation, Formal analysis, Data curation, Conceptualization. **Natalia Málaga:** Writing – review & editing, Writing – original draft, Methodology, Investigation, Formal analysis, Data curation, Conceptualization. **Sean P. Healey:** Writing – review & editing, Methodology, Investigation, Formal analysis, Data curation, Conceptualization. **Robert E. Kennedy:** Writing – review & editing, Writing – original draft, Methodology, Investigation, Formal analysis, Data curation, Conceptualization. **Andrew T. Hudak:** Writing – review & editing, Writing – original draft, Methodology, Investigation, Formal analysis, Data curation, Conceptualization. **Laura Duncanson:** Writing – review & editing, Writing – original draft, Resources, Project administration, Methodology, Investigation, Funding acquisition, Formal analysis, Data curation, Conceptualization.

Declaration of competing interest

The authors declare no competing interests.

Acknowledgments

The research is funded by NASA through the NASA-ESA Multi-mission analysis and algorithm development platform (MAAP) and NASA Carbon Monitoring Systems 2022 (grant 80NSSC23K1255). The contributions of M.H., D.R.S. and N.M. were funded by the ESA Biomass Climate Change Initiative Phase 2 projects and ESA's Global Forests Observations Initiative (GFOI) R&D project. The authors thank Ralph Dubayah (University of Maryland), Sylvia N. Wilson (United States Geological Survey, SilvaCarbon), Javier Garcia-Perez Gamarra (Food and Agriculture Organization of the United Nations), Joana Melo (Joint Research Centre, European Commission), Ronald McRoberts (University of Minnesota) and Erik Næsset (Norwegian University of Life Sciences) for reviewing the article and providing valuable comments on the work.

Code availability

Data was processed on the NASA-ESA Multi-mission Algorithm and Analysis Platform (MAAP), which has public code repositories. The associated code for this article is based in 'R' language and includes scripts for the geostatistical model fitting and the prediction of above-ground biomass. It can be accessed in the NASA MAAP Github repository and is published in Hunka and May (2024).

Appendix

We utilized Gaussian processes to depict spatial variations in the model. A Gaussian process assumes that for any finite set of locations, the process at those locations is multivariate normal. The process is therefore fully defined by its mean and covariance. We assume all Gaussian processes to be mean zero, allowing the intercept and regression to dictate systematic means. The covariance is given by a covariance function, which for any two locations returns the covariance of the process between those locations. We used the Matérn covariance function of smoothness 1 for all Gaussian processes. Using $\tilde{\alpha}(s)$ for exposition, we have

$$\mathrm{Cov}\left(\tilde{\alpha}(s), \tilde{\alpha}(s')\right) = C_\alpha(s, s'), \quad \text{where}$$

$$C_\alpha(s, s') = \sigma_\alpha^2 \sqrt{8}\, \frac{\|s - s'\|}{\phi}\, K_1\left(\sqrt{8}\, \frac{\|s - s'\|}{\phi}\right) \tag{14}$$

where σ_α^2 is the variance parameter and ϕ_α is the range of the spatial process (as in Fig. 4b), for both of which weak prior distributions were supplied during model fitting. $K_1(\cdot)$ is an order 1 modified Bessel function of the second kind. The above equation is opaque, but essentially represents a psuedo-exponential decay with distance between the locations

$$C_\alpha(s, s') \approx \sigma_\alpha^2 \exp\left(-\frac{\|s - s'\|}{\phi_\alpha}\right). \tag{15}$$

The more involved specification in Eq. (14) simply adjusts the behavior of near-zero distances, attenuating the precipitous drop in correlation moving from zero distance, $s = s'$, to slightly positive distances.

For any finite set of n locations, we have

$$\begin{bmatrix} \tilde{\alpha}(s_1) \\ \vdots \\ \tilde{\alpha}(s_n) \end{bmatrix} \sim \mathrm{MVN}(\mathbf{0}, \boldsymbol{\Sigma}) \tag{16}$$

where $[\boldsymbol{\Sigma}]_{ij} = C_\alpha(s_i, s_j)$. The ability of the covariance function to provide covariances between arbitrary locations allows us to predict the process at unobserved locations by leveraging the covariance between the NFI plot locations and the desired prediction locations. Interested readers are referred to Gelfand and Schliep (2016) for a full exposition on Gaussian processes and their use in spatial statistics.

Appendix B. Supplementary data

Supplementary material related to this article can be found online at https://doi.org/10.1016/j.rse.2024.114557.

Data availability

I will provide data and source code openly upon acceptance of article.

References

Babcock, C., Finley, A.O., Andersen, H.E., Pattison, R., Cook, B.D., Morton, D.C., Alonzo, M., Nelson, R., Gregoire, T., Ene, L., Gobakken, T., Næsset, E., 2018. Geostatistical estimation of forest biomass in interior Alaska combining Landsat-derived tree cover, sampled airborne lidar and field observations. Remote Sens. Environ. 212, 212–230. http://dx.doi.org/10.1016/j.rse.2018.04.044.

Babcock, C., Finley, A.O., Bradford, J.B., Kolka, R., Birdsey, R., Ryan, M.G., 2015. Lidar based prediction of forest biomass using hierarchical models with spatially varying coefficients. Remote Sens. Environ. 169, 113–127. http://dx.doi.org/10.1016/j.rse.2015.07.028.

Börner J. West, T., Blackman, A., Miteva, D., Sims, K., Wunder, S., 2018. National and Subnational Forest Conservation Policies: What Works, What Doesn'T. pp. 105–116.

Braden, D., Mondal, P., Park, T., De la rosa, J., Leal, M., Lara, R., Saucedo, R., Salas-Aguilar, V., Soriano-Luna, M., Vargas, R., 2024. Satellite-derived forest extent likelihood map for Mexico. http://dx.doi.org/10.3334/ORNLDAAC/2320, URL: https://daac.ornl.gov/cgi-bin/dsviewer.pl?ds_id=2320.

Breidenbach, J., Ivanovs, J., Kangas, A., Nord-Larsen, T., Nilsson, M., Astrup, R., 2021. Improving living biomass C-stock loss estimates by combining optical satellite, airborne laser scanning, and NFI data. Can. J. Forest Res. 51, 1472–1485. http://dx.doi.org/10.1139/cjfr-2020-0518.

CONABIO, 2008. Ecorregiones terrestres de México (2008) Catálogo de metadatos geográficos. Comisión Nacional para el Conocimiento y Uso de la Biodiversidad. Instituto Nacional de Estadística, Geografía e Informática (INEGI) -Comisión Nacional para el Conocimiento y Uso de la Biodiversidad (CONABIO) - Instituto Nacional de Ecología (INE), URL: http://geoportal.conabio.gob.mx/metadatos/doc/html/ecort08gw.html. Accessed: 2024-04-11.

CONABIO CONANP, 2024. Áreas Naturales Protegidas Federales de México, modificado para el geoportal del SNIB (Fecha de publicación: 10-01-2024, del metadato 10-01-2024). Comisión Nacional para el Conocimiento y Uso de la Biodiversidad (CONABIO), URL: http://geoportal.conabio.gob.mx/metadatos/doc/html/anpmx.html. Accessed: 2024-04-11.

CONAFOR, 2017. Inventario Nacional Forestal y de Suelos Procedimientos de muestreo. Comisión Nacional Forestal, URL: https://www.conafor.gob.mx/apoyos/docs/externos/2022/DocumentosMetodologicos/2019/ANEXO_Procedimientos_de_muestreo_2019.pdf. Accessed: 2024-04-11.

Cressie, N., 2015. Statistics for Spatial Data, revised ed. Probability & Mathematical Statistics S, John Wiley & Sons.

David, F.N., Johnson, N.L., 1948. The probability integral transformation when parameters are estimated from the sample. Biometrika 35, 182. http://dx.doi.org/10.2307/2332638.

Dubayah, R., Armston, J., Kellner, J., Duncanson, L., Healey, S., Patterson, P., Hancock, S., Tang, H., Bruening, J., Hofton, M., Blair, J., Luthcke, S., 2022a. GEDI L4A Footprint Level Aboveground Biomass Density, Version 2.1. ORNL Distributed Active Archive Center, http://dx.doi.org/10.3334/ORNLDAAC/2056.

Dubayah, R., Blair, J.B., Goetz, S., Fatoyinbo, L., Hansen, M., Healey, S., Hofton, M., Hurtt, G., Kellner, J., Luthcke, S., Armston, J., Tang, H., Duncanson, L., Hancock, S., Jantz, P., Marselis, S., Patterson, P.L., Qi, W., Silva, C., 2020. The Global Ecosystem Dynamics Investigation: High-resolution laser ranging of the Earth's forests and topography. Science of Remote Sensing 1, 100002. http://dx.doi.org/10.1016/j.srs.2020.100002, URL: https://www.sciencedirect.com/science/article/pii/S2666017220300018.

Dubayah, R., Hofton, M., Blair, J., Armston, J., Tang, H., Luthcke, S., 2021. GEDI L2A elevation and height metrics data global footprint level V002. http://dx.doi.org/10.5067/GEDI/GEDI02_A.002, URL: https://lpdaac.usgs.gov/products/gedi02_av002/.

Dumelle, M., Higham, M., Ver Hoef, J.M., Olsen, A.R., Madsen, L., 2022. A comparison of design-based and model-based approaches for finite population spatial sampling and inference. Methods Ecol. Evol. 13, 2018–2029. http://dx.doi.org/10.1111/2041-210x.13919.

Duncanson, L., Kellner, J.R., Armston, J., Dubayah, R., Minor, D.M., Hancock, S., Healey, S.P., Patterson, P.L., Saarela, S., Marselis, S., Silva, C.E., Bruening, J., Goetz, S.J., Tang, H., Hofton, M., Blair, B., Luthcke, S., Fatoyinbo, L., Abernethy, K., Alonso, A., Andersen, H.E., Aplin, P., Baker, T.R., Barbier, N., Bastin, J.F., Biber, P., Boeckx, P., Bogaert, J., Boschetti, L., Boucher, P.B., Boyd, D.S., Burslem, D.F., Calvo-Rodriguez, S., Chave, J., Chazdon, R.L., Clark, D.B., Clark, D.A., Cohen, W.B., Coomes, D.A., Corona, P., Cushman, K., Cutler, M.E., Dalling, J.W., Dalponte, M., Dash, J., de Miguel, S., Deng, S., Ellis, P.W., Erasmus, B., Fekety, P.A., Fernandez-Landa, A., Ferraz, A., Fischer, R., Fisher, A.G., García-Abril, A., Gobakken, T., Hacker, J.M., Heurich, M., Hill, R.A., Hopkinson, C., Huang, H., Hubbell, S.P., Hudak, A.T., Huth, A., Imbach, B., Jeffery, K.J., Katoh, M., Kearsley, E., Kenfack, D., Kljun, N., Knapp, N., Král, K., Krůček, M., Labrière, N., Lewis, S.L., Longo, M., Lucas, R.M., Main, R., Manzanera, J.A., Martínez, R.V., Mathieu, R., Memiaghe, H., Meyer, V., Mendoza, A.M., Monerris, A., Montesano, P., Morsdorf, F., Næsset, E., Naidoo, L., Nilus, R., O'Brien, M., Orwig, D.A., Papathanassiou, K., Parker, G., Philipson, C., Phillips, O.L., Pisek, J., Poulsen, J.R., Pretzsch, H., Rüdiger, C., Saatchi, S., Sanchez-Azofeifa, A., Sanchez-Lopez, N., Scholes, R., Silva, C.A., Simard, M., Skidmore, A., Stereńczak, K., Tanase, M., Torresan, C., Valbuena, R., Verbeeck, H., Vrska, T., Wessels, K., White, J.C., White, L.J., Zahabu, E., Zgraggen, C., 2022. Aboveground biomass density models for NASA's Global Ecosystem Dynamics Investigation (GEDI) lidar mission. Remote Sens. Environ. 270, 112845. http://dx.doi.org/10.1016/j.rse.2021.112845, URLprefix https://www.sciencedirect.com/science/article/pii/S0034425721005654.

EDGE, 2024. Earth Dynamics Geodetic Explorer: A competitive Phase A Concept Study within NASA's Earth Systems Explorer (ESE). URL: https://edge.ucsd.edu/.

Ekström, M., Nilsson, M., 2021. A comparison of model-assisted estimators, with and without data-driven transformations of auxiliary variables, with application to forest inventory. Front. Forests Global Change 4, http://dx.doi.org/10.3389/ffgc.2021.764495.

Emick, E., Babcock, C., White, G.W., Hudak, A.T., Domke, G.M., Finley, A.O., 2023. An approach to estimating forest biomass while quantifying estimate uncertainty and correcting bias in machine learning maps. Remote Sens. Environ. 295, 113678. http://dx.doi.org/10.1016/j.rse.2023.113678.

Fassnacht, F.E., White, J.C., Wulder, M.A., Næsset, E., 2023. Remote sensing in forestry: current challenges, considerations and directions. Forestry: Int. J. Forest Res. 97, 11–37. http://dx.doi.org/10.1093/forestry/cpad024.

GCOS, 2022. Global Climate Observing System: The 2022 GCOS ECVs Requirements (GCOS 245). Technical Report.

Gelfand, A.E., Schliep, E.M., 2016. Spatial statistics and Gaussian processes: A beautiful marriage. Spat. Stat. 18, 86–104. http://dx.doi.org/10.1016/j.spasta.2016.03.006.

GFOI, 2020. Integration of remote-sensing and ground-based observations for estimation of emissions and removals of greenhouse gases in forests. In: Methods and Guidance from the Global Forest Observations Initiative (GFOI). Edition 3.0. http://dx.doi.org/10.1201/9781315175584, URL: https://www.reddcompass.org/mgd/resources/GFOI-MGD-3.1-en.pdf. Bayesian Inference with INLA.

Gómez Rubio, V., 2020. Bayesian Inference with INLA. http://dx.doi.org/10.1201/9781315175584.

Heaton, M.J., Datta, A., Finley, A.O., Furrer, R., Guinness, J., Guhaniyogi, R., Gerber, F., Gramacy, R.B., Hammerling, D., Katzfuss, M., et al., 2019. A case study competition among methods for analyzing large spatial data. J. Agric. Biol. Environ. Stat. 24, 398–425. http://dx.doi.org/10.1007/s13253-018-00348-w.

Held, L., Schrödle, B., Rue, H., 2010. Posterior and Cross-Validatory Predictive Checks: A Comparison of MCMC and INLA. Physica-Verlag HD, Heidelberg, pp. 91–110. http://dx.doi.org/10.1007/978-3-7908-2413-1_6.

Herold, M., Carter, S., Avitabile, V., Espejo, A.B., Jonckheere, I., Lucas, R., McRoberts, R.E., Næsset, E., Nightingale, J., Petersen, R., Reiche, J., Romijn, E., Rosenqvist, A., Rozendaal, D.M.A., Seifert, F.M., Sanz, M.J., De Sy, V., 2019. The role and need for space-based forest biomass-related measurements in environmental management and policy. Surv. Geophys. 40, 757–778. http://dx.doi.org/10.1007/s10712-019-09510-6.

Hunka, N., May, P., 2024. Geostatistical approach: National forest biomass assessments enhanced with Earth Observation to aid climate policy needs. http://dx.doi.org/10.5281/zenodo.14003423.

Hunka, N., Santoro, M., Armston, J., Dubayah, R., McRoberts, R.E., Næsset, E., Quegan, S., Urbazaev, M., Pascual, A., May, P.B., Minor, D., Leitold, V., Basak, P., Liang, M., Melo, J., Herold, M., Málaga, N., Wilson, S., Durán Montesinos, P., Arana, A., Ernesto De La Cruz Paiva, R., Ferrand, J., Keoka, S., Guerra-Hernández, J., Duncanson, L., 2023. On the NASA GEDI and ESA CCI biomass maps: aligning for uptake in the UNFCCC global stocktake. Environ. Res. Lett. 18, 124042. http://dx.doi.org/10.1088/1748-9326/ad0b60.

INEGI, 2020. Marco Geoestadístico. Censo de Población y Vivienda 2020. Instituto Nacional de Estadística, Geografía e Informática (INEGI), URL: https://www.inegi.org.mx/app/biblioteca/ficha.html?upc=889463807469. Accessed: 2024-04-11.

INFyS, 2024. Inventario Nacional Forestal y de Suelos Procedimientos de muestreo. Comisión Nacional Forestal, URL: https://snmf.cnf.gob.mx/infys/. Accessed: 2024-04-11.

IPCC, 2006. 2006 IPCC Guidelines for National Greenhouse Gas Inventories. In: Agriculture, Forestry and Other Land Use, vol. 4, URL: http://www.ipcc-nggip.iges.or.jp/public/2006gl/index.html.

IPCC, 2019. Refinement to the 2006 IPCC Guidelines for National Greenhouse Gas Inventories. Chapter 4: Forest Land. URL https://www.ipcc-nggip.iges.or.jp/public/2019rf/pdf/4_Volume4/19R_V4_Ch04_Forest%20Land.pdf.

JAXA, 2024. Advanced Land Observing Satellite-4 DAICHI-4 (ALOS-4): In Opertation. URL: https://global.jaxa.jp/projects/sat/alos4/. Accessed: 2024-10-28.

Johnson, K.D., Birdsey, R., Finley, A.O., Swantaran, A., Dubayah, R., Wayson, C., Riemann, R., 2014. Integrating forest inventory and analysis data into a lidar-based carbon monitoring system. Carbon Balance Manage. 9, http://dx.doi.org/10.1186/1750-0680-9-3.

Lang, N., Jetz, W., Schindler, K., Wegner, J.D., 2023. A high-resolution canopy height model of the earth. Nat. Ecol. Evol. 7, 1778–1789. http://dx.doi.org/10.1038/s41559-023-02206-6.

Lefsky, M.A., Cohen, W.B., Parker, G.G., Harding, D.J., 2002. Lidar remote sensing for ecosystem studies. BioScience 52 (19), http://dx.doi.org/10.1641/0006-3568(2002)052[0019:lrsfes]2.0.co;2.

Lindgren, F., Rue, H., 2015. Bayesian spatial modelling with R-INLA. J. Stat. Softw. 63, 1–25. http://dx.doi.org/10.18637/jss.v063.i19, URL: https://www.jstatsoft.org/index.php/jss/article/view/v063i19.

Lindgren, F., Rue, H., Lindström, J., 2011. An explicit link between Gaussian fields and Gaussian Markov random fields: the stochastic partial differential equation approach. J. R. Stat. Soc. Ser. B Stat. Methodol. 73, 423–498. http://dx.doi.org/10.1111/j.1467-9868.2011.00777.x.

Málaga, N., de Bruin, S., McRoberts, R.E., Arana Olivos, A., de la Cruz Paiva, R., Durán Montesinos, P., Requena Suarez, D., Herold, M., 2022. Precision of subnational forest AGB estimates within the Peruvian Amazonia using a global biomass map. Int. J. Appl. Earth Obs. Geoinf. 115, 103102. http://dx.doi.org/10.1016/j.jag.2022.103102, URL: https://www.sciencedirect.com/science/article/pii/S1569843222002904.

Markus, T., Neumann, T., Martino, A., Abdalati, W., Brunt, K., Csatho, B., Farrell, S., Fricker, H., Gardner, A., Harding, D., Jasinski, M., Kwok, R., Magruder, L., Lubin, D., Luthcke, S., Morison, J., Nelson, R., Neuenschwander, A., Palm, S., Popescu, S., Shum, C., Schutz, B.E., Smith, B., Yang, Y., Zwally, J., 2017. The Ice, Cloud, and land Elevation Satellite-2 (ICESat-2): Science requirements, concept, and implementation. Remote Sens. Environ. 190, 260–273. http://dx.doi.org/10.1016/j.rse.2016.12.029, URL: https://www.sciencedirect.com/science/article/pii/S0034425716305089.

Matérn, B., 1960. Spatial variation : Stochastic models and their application to some problems in forest surveys and other sampling investigations. URL: https://api.semanticscholar.org/CorpusID:127177440.

May, P.B., Dubayah, R.O., Bruening, J.M., Gaines, G.C., 2024. Connecting spaceborne lidar with NFI networks: A method for improved estimation of forest structure and biomass. Int. J. Appl. Earth Obs. Geoinf. 129, 103797. http://dx.doi.org/10.1016/j.jag.2024.103797.

May, P., McConville, K.S., Moisen, G.G., Bruening, J., Dubayah, R., 2023. A spatially varying model for small area estimates of biomass density across the contiguous United States. Remote Sens. Environ. 286, 113420. http://dx.doi.org/10.1016/j.rse.2022.113420, URL: https://www.sciencedirect.com/science/article/pii/S0034425722005260.

McRoberts, R.E., 2010. Probability- and model-based approaches to inference for proportion forest using satellite imagery as ancillary data. Remote Sens. Environ. 114, 1017–1025. http://dx.doi.org/10.1016/j.rse.2009.12.013.

McRoberts, R.E., Næsset, E., Gobakken, T., 2014. Estimation for inaccessible and non-sampled forest areas using model-based inference and remotely sensed auxiliary information. Remote Sens. Environ. 154, 226–233. http://dx.doi.org/10.1016/j.rse.2014.08.028.

McRoberts, R.E., Næsset, E., Saatchi, S., Liknes, G.C., Walters, B.F., Chen, Q., 2019. Local validation of global biomass maps. Int. J. Appl. Earth Obs. Geoinf. 83, 101931. http://dx.doi.org/10.1016/j.jag.2019.101931, URL: https://www.sciencedirect.com/science/article/pii/S0303243419305033.

McRoberts, R.E., Næsset, E., Saatchi, S., Quegan, S., 2022. Statistically rigorous, model-based inferences from maps. Remote Sens. Environ. 279, 113028. http://dx.doi.org/10.1016/j.rse.2022.113028, URL: https://www.sciencedirect.com/science/article/pii/S0034425722001420.

McRoberts, R.E., Westfall, J.A., 2013. Effects of uncertainty in model predictions of individual tree volume on large area volume estimates. Forest Sci. 60, 34–42. http://dx.doi.org/10.5849/forsci.12-141.

Melo, J., Baker, T., Nemitz, D., Quegan, S., Ziv, G., 2023. Satellite-based global maps are rarely used in forest reference levels submitted to the UNFCCC. Environ. Res. Lett. 18, 034021. http://dx.doi.org/10.1088/1748-9326/acba31.

Næsset, E., Gobakken, T., Solberg, S., Gregoire, T.G., Nelson, R., Ståhl, G., Weydahl, D., 2011. Model-assisted regional forest biomass estimation using LiDAR and InSAR as auxiliary data: A case study from a boreal forest area. Remote Sens. Environ. 115, 3599–3614. http://dx.doi.org/10.1016/j.rse.2011.08.021, URL: https://www.sciencedirect.com/science/article/pii/S0034425711003257.

NASA, 2010. Carbon monitoring system, national aeronautics and space administration. URL: https://carbon.nasa.gov/cms/ [accessed: 2024-04-11].

NASA, 2021. Biomass Earthdata Dashboard BETA: The Biomass Harmonization Activity. URL: https://www.earthdata.nasa.gov/maap-biomass/.

NASA-JPL, 2019. NASA-ISRO SAR (NISAR) Mission Science Users' Handbook. URL: https://nisar.jpl.nasa.gov/documents/26/NISAR_FINAL_9-6-19.pdf. Accessed: 2024-04-11.

Neeff, T., Piazza, M., 2019. Developing forest monitoring capacity – progress achieved and gaps remaining after ten years. Forest Policy Econ. 101, 88–95. http://dx.doi.org/10.1016/j.forpol.2018.10.013, URL: https://www.sciencedirect.com/science/article/pii/S1389934118304271.

Nesha, K., Herold, M., De Sy, V., de Bruin, S., Araza, A., Málaga, N., Gamarra, J.G., Hergoualc'h, K., Pekkarinen, A., Ramirez, C., Morales-Hidalgo, D., Tavani, R., 2022. Exploring characteristics of national forest inventories for integration with global space-based forest biomass data. Sci. Total Environ. 850, 157788. http://

dx.doi.org/10.1016/j.scitotenv.2022.157788, URL: https://www.sciencedirect.com/science/article/pii/S0048969722048872.

Potapov, P., Li, X., Hernandez-Serna, A., Tyukavina, A., Hansen, M.C., Kommareddy, A., Pickens, A., Turubanova, S., Tang, H., Silva, C.E., Armston, J., Dubayah, R., Blair, J.B., Hofton, M., 2021. Mapping global forest canopy height through integration of GEDI and Landsat data. Remote Sens. Environ. 253, 112165. http://dx.doi.org/10.1016/j.rse.2020.112165, URL: https://www.sciencedirect.com/science/article/pii/S0034425720305381.

Qi, W., Armston, J., Choi, C., Stovall, A., Saarela, S., Pardini, M., Fatoyinbo, L., Papathanasiou, K., Dubayah, R., 2023. Mapping Large-Scale Pantropical Forest Canopy Height By Integrating GEDI Lidar and TanDEM-X InSAR Data. http://dx.doi.org/10.21203/rs.3.rs-3306982/v1.

Quegan, S., Le Toan, T., Chave, J., Dall, J., Exbrayat, J.F., Minh, D.H.T., Lomas, M., D'Alessandro, M.M., Paillou, P., Papathanassiou, K., Rocca, F., Saatchi, S., Scipal, K., Shugart, H., Smallman, T.L., Soja, M.J., Tebaldini, S., Ulander, L., Villard, L., Williams, M., 2019. The European Space Agency BIOMASS mission: Measuring forest above-ground biomass from space. Remote Sens. Environ. 227, 44–60. http://dx.doi.org/10.1016/j.rse.2019.03.032, URL: https://www.sciencedirect.com/science/article/pii/S0034425719301233.

R Core Team, 2022. R: A Language and Environment for Statistical Computing. R Foundation for Statistical Computing, Vienna, Austria, URL: https://www.R-project.org/.

Rao, S.S., 2017. The Finite Element Method in Engineering. Butterworth-heinemann, http://dx.doi.org/10.1016/C2009-0-04807-7.

Réjou-Méchain, M., Barbier, N., Couteron, P., Ploton, P., Vincent, G., Herold, M., Mermoz, S., Saatchi, S., Chave, J., Boissieu, F.de., Féret, J.B., Takoudjou, S.M., Pélissier, R., 2019. Upscaling forest biomass from field to satellite measurements: Sources of errors and ways to reduce them. Surv. Geophys. 40, 881–911. http://dx.doi.org/10.1007/s10712-019-09532-0.

Romijn, E., Herold, M., Kooistra, L., Murdiyarso, D., Verchot, L., 2012. Assessing capacities of non-Annex I countries for national forest monitoring in the context of REDD+. Environ. Sci. Policy 19–20, 33–48. http://dx.doi.org/10.1016/j.envsci.2012.01.005.

Saarela, S., Holm, S., Healey, S.P., Andersen, H.E., Petersson, H., Prentius, W., Patterson, P.L., Næsset, E., Gregoire, T.G., Ståhl, G., 2018. Generalized hierarchical model-based estimation for aboveground biomass assessment using GEDI and landsat data. Remote Sens. 10, http://dx.doi.org/10.3390/rs10111832, URL: https://www.mdpi.com/2072-4292/10/11/1832.

Santoro, M., Cartus, O., 2023. ESA Biomass Climate Change Initiative (Biomass_cci): Global datasets of forest above-ground biomass for the years 2010 2017, 2018 2019 and 2020, v4. URL: https://catalogue.ceda.ac.uk/uuid/af60720c1e404a9e9d2c145d2b2ead4e.

Santoro, M., Cartus, O., Carvalhais, N., Rozendaal, D.M.A., Avitabile, V., Araza, A., de Bruin, S., Herold, M., Quegan, S., Rodríguez-Veiga, H., Carreiras, J., Schepaschenko, D., Korets, M., Shimada, M., Itoh, T., Moreno Martínez, J., Gatti, R. Cazzolla, da Conceição Bispo, N., Labrière, N., Liang, J., Lindsell, J., Mitchard, E.T.A., Morel, A., Pacheco Pascagaza, A.M., Ryan, C.M., Slik, F., Laurin, G. Vaglio, Verbeeck, H., Wijaya, A., Willcock, S., 2021. The global forest above-ground biomass pool for 2010 estimated from high-resolution satellite observations. Earth Syst. Sci. Data 13, 3927–3950. http://dx.doi.org/10.5194/essd-13-3927-2021, URL: https://essd.copernicus.org/articles/13/3927/2021/.

Santoro, M., Cartus, O., Quegan, S., Kay, H., Lucas, R.M., Araza, A., Herold, M., Labrière, N., Chave, J., Rosenqvist, Åke, Tadono, T., Kobayashi, K., Kellndorfer, J., Avitabile, V., Brown, H., Carreiras, J., Campbell, M.J., Cavlovic, J., da Conceição Bispo, P., Gilani, H., Khan, M.L., Kumar, A., Lewis, S.L., Liang, J., Mitchard, E.T., Pacheco-Pascagaza, A.M., Phillips, O.L., Ryan, C.M., Saikia, P., Schepaschenko, D., Sukhdeo, H., Verbeeck, H., Vieilledent, G., Wijaya, A., Willcock, S., Seifert, F.M., 2024. Design and performance of the climate change initiative biomass global retrieval algorithm. Sci. Remote Sensing 10, 100169. http://dx.doi.org/10.1016/j.srs.2024.100169, URL: https://www.sciencedirect.com/science/article/pii/S2666017224000531.

Schroeder, T.A., Healey, S.P., Moisen, G.G., 2012. Evaluating the compatibility of American and mexican national forest inventory data. In: McWilliams, Will, Roesch, Francis A. (Eds.), Monitoring Across Borders: 2010 Joint Meeting of the Forest Inventory and Analysis (FIA) Symposium and the Southern Mensurationists. e-Gen. Tech. Rep. SRS-157, U.S. Department of Agriculture Forest Service, Southern Research Station, Asheville, NC, pp. 15–22. http://dx.doi.org/10.2737/SRS-GTR-157.

Ståhl, G., Gobakken, T., Saarela, S., Persson, H.J., Ekström, M., Healey, S.P., Yang, Z., Holmgren, J., Lindberg, E., Nyström, K., Papucci, E., Ulvdal, P., Ørka, H.O., Næsset, E., Hou, Z., Olsson, H., McRoberts, R.E., 2024. Why ecosystem characteristics predicted from remotely sensed data are unbiased and biased at the same time – and how this affects applications. Forest Ecosystems 11, 100164. http://dx.doi.org/10.1016/j.fecs.2023.100164, URL: https://www.sciencedirect.com/science/article/pii/S2197562023000957.

Ståhl, G., Saarela, S., Schnell, S., Holm, S., Breidenbach, J., Healey, S.P., Patterson, P.L., Magnussen, S., Næsset, E., McRoberts, R.E., Gregoire, T.G., 2016. Use of models in large-area forest surveys: comparing model-assisted, model-based and hybrid estimation. Forest Ecosyst. 3, http://dx.doi.org/10.1186/s40663-016-0064-9.

Streck, C., 2021. How voluntary carbon markets can drive climate ambition. J. Energy Nat. Resour. Law 39, 367–374. http://dx.doi.org/10.1080/02646811.2021.1881275.

Tomppo, E., Gschwantner, T., Lawrence, M., McRoberts, R.E., 2010. National Forest Inventories: Pathways for Common Reporting. Springer Netherlands, http://dx.doi.org/10.1007/978-90-481-3233-1.

UNFCCC, 2014. The Warsaw Framework for REDD-Plus Decisions 9–12/CP.19 Report No. FCCC/CP/2013/10/Add.1. Technical Report, United Nations Framework Convention on Climate Change.

UNFCCC, 2015. Decision 19/CMA.1: Adoption of the Paris Agreement Report No. FCCC/CP/2015/L.9/Rev.1. Technical Report, United Nations Framework Convention on Climate Change, Paris.

Urbazaev, M., Thiel, C., Cremer, F., Dubayah, R., Migliavacca, M., Reichstein, M., Schmullius, C., 2018. Estimation of forest aboveground biomass and uncertainties by integration of field measurements, airborne LiDAR, and SAR and optical satellite data in Mexico. Carbon Balance Manage. 13, http://dx.doi.org/10.1186/s13021-018-0093-5.

USGS, 2012. U.S. Geological Survey, SilvaCarbon. URL: https://www.usgs.gov/silvacarbon/.

Velasco Bautista, E., Maldonado, H. Ramírez, Sánchez, F. Moreno, de la Rosa Vázquez, A., 2020. Estimadores De Razón Para El Inventario Nacional Forestal De México. Revista Mexicana de Ciencias Forestales 28, 23–43, URL: http://cienciasforestales.inifap.gob.mx/index.php/forestales/article/view/882.

Wilkinson, M.D., Dumontier, M., Aalbersberg, I.J., Appleton, G., Axton, M., Baak, A., Blomberg, N., Boiten, J.W., da Silva Santos, L.B., Bourne, P.E., Bouwman, J., Brookes, A.J., Clark, T., Crosas, M., Dillo, I., Dumon, O., Edmunds, S., Evelo, C.T., Finkers, R., Gonzalez-Beltran, A., Gray, A.J., Groth, P., Goble, C., Grethe, J.S., Heringa, J., 't Hoen, P.A., Hooft, R., Kuhn, T., Kok, R., Kok, J., Lusher, S.J., Martone, M.E., Mons, A., Packer, A.L., Persson, B., Rocca-Serra, P., Roos, M., van Schaik, R., Sansone, S.A., Schultes, E., Sengstag, T., Slater, T., Strawn, G., Swertz, M.A., Thompson, M., van der Lei, J., van Mulligen, E., Velterop, J., Waagmeester, A., Wittenburg, P., Wolstencroft, K., Zhao, J., Mons, B., 2016. The FAIR Guiding Principles for scientific data management and stewardship. Sci. Data 3, 160018. http://dx.doi.org/10.1038/sdata.2016.18.

Wulder, M.A., Bater, C.W., Coops, N.C., Hilker, T., White, J.C., 2008. The role of LiDAR in sustainable forest management. For. Chron 84, 807–826. http://dx.doi.org/10.5558/tfc84807-6.

Zienkiewicz, O.C., Taylor, R.L., Zhu, J.Z., 2005. The Finite Element Method: Its Basis and Fundamentals. Elsevier, http://dx.doi.org/10.1016/C2009-0-24909-9.